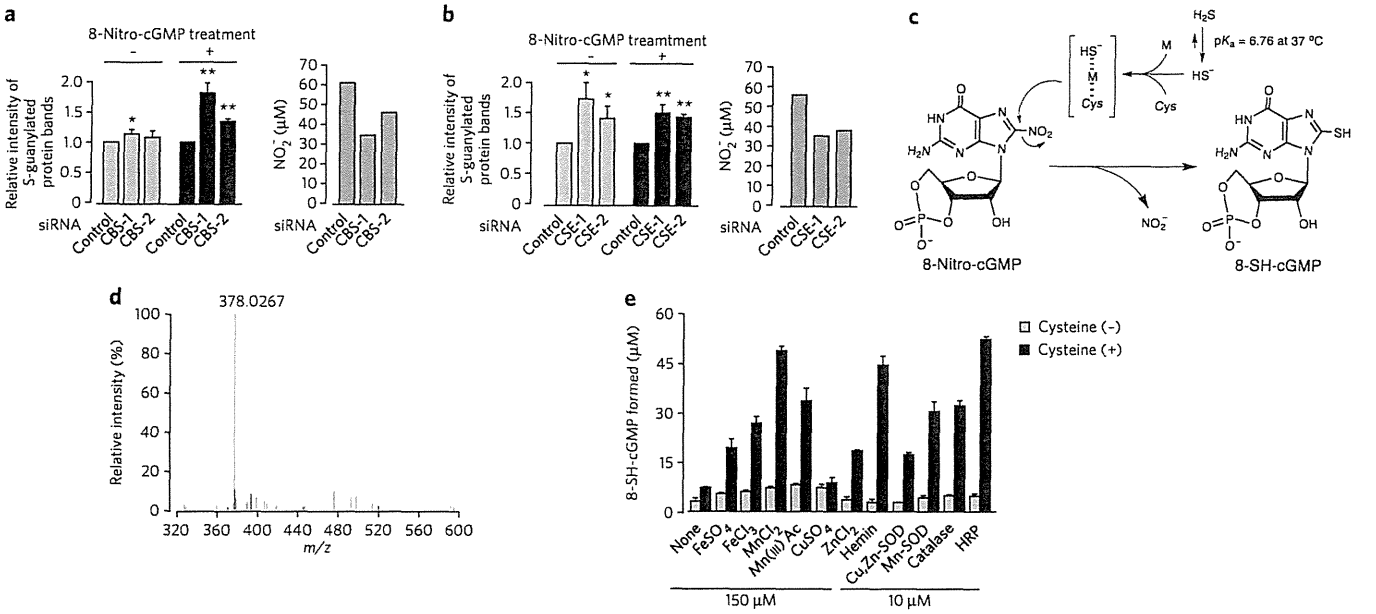

Figure 1 | Regulation of 8-nitro-cGMP-induced protein S-guanylation by HS^--producing enzymes via sulfhydration of 8-nitro-cGMP by HS^-. (**a**,**b**) Enhancement of protein S-guanylation by knockdown of CBS (**a**) and CSE (**b**) in A549 cells treated or untreated with 8-nitro-cGMP (200 μM). In **a** and **b**, quantitative data (via densitometric analysis) of S-guanylation western blots are shown at left, and NO_2^- release from 8-nitro-cGMP with A549 cells in culture with and without knockdown of CBS or CSE is shown at right. Data represent mean ± s.e.m. (n = 4). *P < 0.05, **P < 0.01 versus control. Original western blot images are shown in **Supplementary Figure 1b**. (**c**) Possible reaction mechanisms in HS^--dependent sulfhydration of 8-nitro-cGMP. Transition metals (M) and cysteine thiolate anion (Cys-S^-) may participate in sulfhydration by stabilizing the HS^- anion. (**d**) Mass spectrum of the peak identified as 8-SH-cGMP formed in the reaction of 8-nitro-cGMP with NaHS. (**e**) Effects of cysteine and metals on HS^--mediated sulfhydration of 8-nitro-cGMP. The reaction of 8-nitro-cGMP (100 μM) with NaHS (1 mM) was carried out in 100 mM sodium phosphate buffer (pH 7.4) containing 100 μM DTPA in the absence or presence of additives including cysteine (100 μM), metals (150 μM $FeSO_4$, $FeCl_3$, $MnCl_2$, $CuSO_4$ or $ZnCl_2$) and metal-containing compounds or proteins (10 μM hemin, Cu,Zn-SOD, Mn-SOD, catalase or HRP) at 37 °C for 5 h. Data represent mean ± s.d. (n = 3).

based on the modulation of protein S-guanylation in A549 (human lung epithelial adenocarcinoma) and other cultured cells after treatment with small interfering RNA (siRNA) for various genes (**Fig. 1a,b**). This RNAi screening revealed the substantial impact of endogenous HS^- generation on 8-nitro-cGMP metabolism. In particular, two key enzymes of HS^--H_2S biosynthesis, cystathionine β-synthase (CBS) and cystathionine γ-lyase (CSE) (**Supplementary Fig. 1a**), had a significant impact on the metabolism of cellular 8-nitro-cGMP in cultured mammalian cell lines, including A549, HepG2 (human hepatoblastoma) and C6 cells (rat glioblastoma) (P < 0.05 or P < 0.01 for each assay; **Fig. 1a,b** and **Supplementary Fig. 1**). Protein S-guanylation caused by exogenously administered 8-nitro-cGMP was markedly augmented after knockdown of CBS or CSE in A549, HepG2 and C6 cells (**Fig. 1a,b** and **Supplementary Fig. 1b–d**). Moreover, the basal extent of protein S-guanylation induced by endogenous 8-nitro-cGMP generation was also elevated by CBS or CSE knockdown (**Fig. 1a,b**). These data reveal that the HS^--generating enzymes (CBS and CSE) are critical for 8-nitro-cGMP metabolism. This metabolism was linked with the release of nitrite (NO_2^-) via a mechanism dependent on CBS and CSE (**Fig. 1a,b** and **Supplementary Figs. 1** and **2**), supporting a reliance on the nucleophilic qualities of H_2S (pK_a 6.7), especially anionic HS^-, which predominates in neutral biological solutions (**Fig. 1c**)[13]. The extent of NO_2^- generation was linked with 8-nitro-cGMP degradation in cells, which in turn depended on HS^- formed from CBS or CSE (**Supplementary Fig. 2b,c**). These findings support that enzymatically generated HS^- mediates 8-nitro-cGMP metabolism.

Denitration and sulfhydration of 8-nitro-cGMP by HS^-

To clarify how HS^-, rather than gaseous H_2S, could undergo an SH-addition reaction (that is, electrophile sulfhydration), we analyzed cell-free reactions of 8-nitro-cGMP with sodium hydrosulfide (NaHS), used as an HS^- donor, via reverse-phase HPLC (RP-HPLC) and LC/MS. The electrophilic nitro moiety underwent nucleophilic substitution with HS^- to yield the new product, 8-SH-cGMP (**Fig. 1c,d** and **Supplementary Fig. 3a**). Transition metal ions such as iron and manganese added to the reaction mixture greatly increased 8-SH-cGMP formation, whereas copper addition showed no or minimal effects (**Fig. 1e**). Metal complexes and metalloproteins, such as hemin, Cu,Zn-superoxide dismutase (Cu,Zn-SOD), Mn-SOD, horseradish peroxidase (HRP) and catalase, also promoted sulfhydration reactions, with HRP having the greatest effect. This observation supports a potent catalytic activity of endogenous transition metals—and metalloproteins—in sulfhydration. Sulfhydryls act as ligands for metal ions; thus, HS^--containing metal complexes may acquire added stability and catalyze sulfhydration (**Fig. 1c**). H_2S can be oxidized to sulfur oxides such as thiosulfate ($S_2O_3^{2-}$), sulfite (SO_3^{2-}) and sulfate (SO_4^{2-}) under aerobic conditions or via cell metabolism[2,14]. These sulfur oxides, which may be formed via oxidation of H_2S/HS^-, did not react with 8-nitro-cGMP to induce sulfhydration (**Supplementary Fig. 3b**), confirming the specificity of HS^- in electrophile sulfhydration. We observed clear pH-dependent, HS^--induced sulfhydration of 8-nitro-cGMP (**Supplementary Fig. 3c**). The efficacy of 8-SH-cGMP formation increased linearly as the pH increased from 5 to 8, which correlated well with the reported pH-dependent equilibrium of H_2S/HS^- (ref. 13). The electrophile sulfhydration potential of HS^- is superior to that of GSH-dependent nucleophilic modification of 8-nitro-cGMP within a physiologically relevant pH range of the reaction mixture containing cysteine and HRP (**Supplementary Fig. 3c**). This finding also indicates a substantial contribution of HS^- to electrophile metabolism via sulfhydration in comparison with electrophile

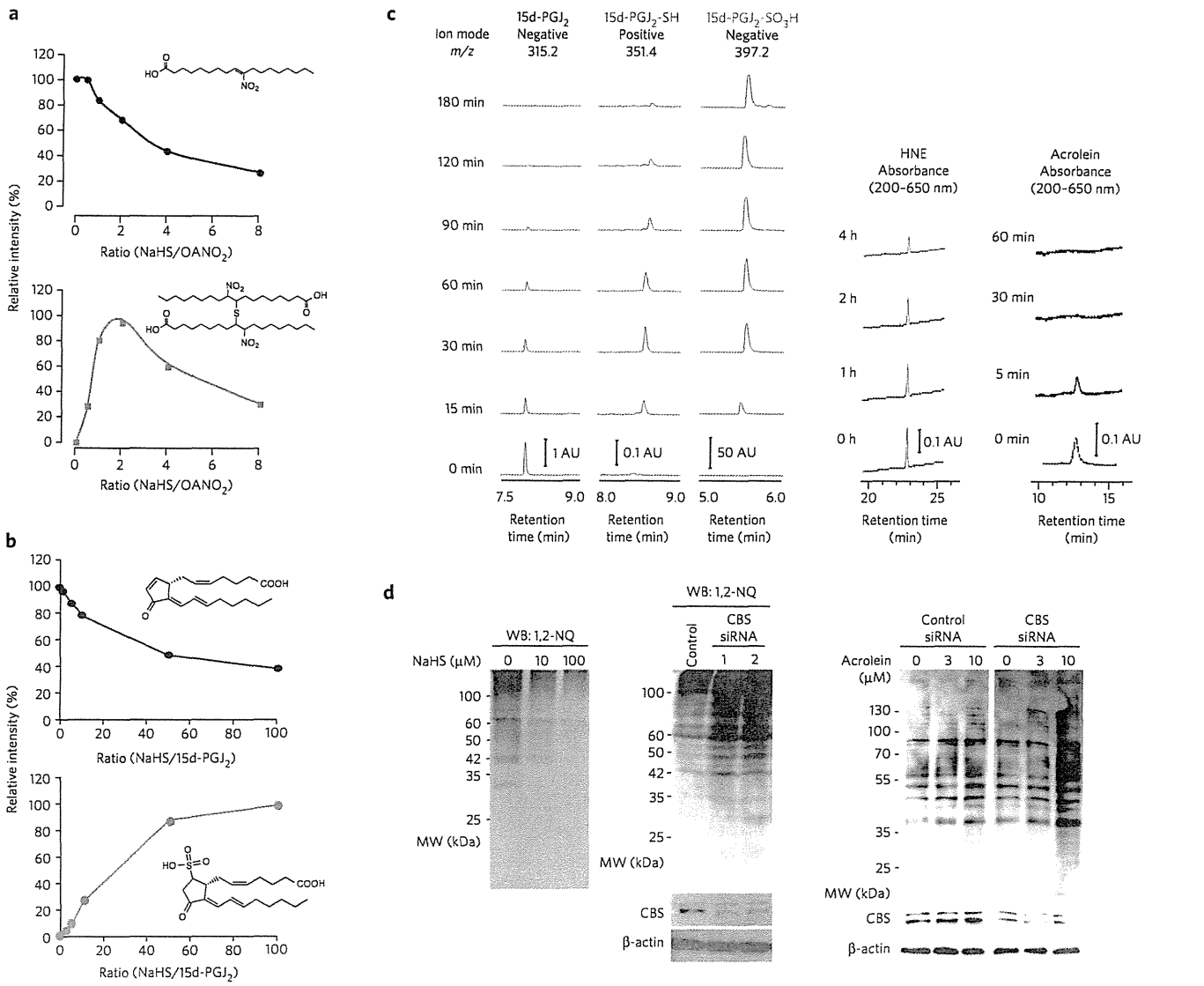

Figure 2 | Electrophile sulfhydration by HS^-. (**a**) LC/MS analysis for the $OANO_2$ and HS^- reaction. $OANO_2$ (100 μM) was reacted with different concentrations of NaHS in 200 mM potassium phosphate buffer at 25 °C for 1 h. (**b**) LC/MS for identification of 15d-PGJ_2-SO_3H as a product of the reaction of 15d-PGJ_2 (1 μM) and HS^- in 100 mM phosphate buffer at 37 °C for 2 h. (**c**) Time-dependent effects of HS^- on stability of various electrophiles. Left, single-ion recordings of 15d-PGJ_2, 15d-PGJ_2-SH and 15d-PGJ_2-SO_3H in the same reaction as in **b** with 15d-PGJ_2 (10 μM) and NaHS (1 mM). The MS spectrum of each PGJ_2 derivative is shown in **Supplementary Figure 4c**. Right, HNE and acrolein determined by RP-HPLC analyses. HNE (10 μM) or acrolein (10 μM) was incubated with NaHS (200 μM for HNE; 100 μM for acrolein) in 100 mM phosphate buffer at 37 °C. AU, arbitrary unit. (**d**) Effects of HS^- on protein electrophile adductions in A549 cells. Cells were pretreated with NaHS or were untreated for 12 h, followed by treatment with 1,2-NQ (10 μM) for 1 h. Total cellular proteins were subjected to western blotting (WB). Cells were transfected with control siRNA or CBS siRNA and were then exposed to 1,2-NQ (10 μM) for 1 h or to acrolein (3 μM or 10 μM) for 30 min. Western blots for 1,2-NQ and acrolein protein adducts formed in A549 cells with CBS knockdown or untreated cells (middle and right). Uncropped blots are shown in **Supplementary Figure 17**. MW, molecular weight.

metabolism with GSH and other sulfhydryl compounds such as cysteine and homocysteine (HCys) with a relatively high pK_a (>8).

HS^--mediated sulfhydration with diverse electrophiles

Sulfhydration by HS^- occurred with a broad array of biological electrophiles that have either cell signaling or toxicological properties (**Fig. 2** and **Supplementary Fig. 4**). These electrophiles include the cyclopentenone 15-deoxy-$\Delta^{12,14}$-prostaglandin J_2 (15d-PGJ_2), 4-hydroxy-2-nonenal (HNE), acrolein and fatty acid nitroalkene derivatives. LC/MS indicated that the common primary reaction with these electrophilic lipid derivatives was nucleophilic addition or substitution of HS^- at the electrophilic carbon (**Figs. 2** and **3** and **Supplementary Fig. 4**). Another reaction was the Michael addition of HS^- to electrophiles such as 1,2-naphthoquinone (1,2-NQ) and other related quinones (**Supplementary Figs. 5** and **6**). The reaction of 1,2-NQ with HS^- yielded 1,2-NQ-SH and $(1,2\text{-NQ})_2S$.

Reactions occurring after sulfhydration varied with individual electrophiles. In many cases, secondary reactions with parent electrophiles yielded bis-thio derivatives, as was observed with nitro-oleic acid ($OANO_2$), which underwent S-bridged dimerization (**Figs. 2a** and **3a** and **Supplementary Fig. 4a,b**), and with 1,2-NQ, 1,4-NQ and *tert*-butylbenzoquinone (**Supplementary Fig. 5**). One exception was 8-nitro-cGMP; RP-HPLC and LC/MS detected only the sulfhydrated product, 8-SH-cGMP. Similarly to 8-nitro-cGMP, 15d-PGJ_2 was readily sulfhydrated to form a transient unstable SH adduct that rapidly converted to sulfonated 15d-PGJ_2-SO_3H, the sole final product (**Figs. 2b,c** and **3a** and **Supplementary Figs. 4c** and **6**). This interpretation is supported by the fate of 8-SH-cGMP

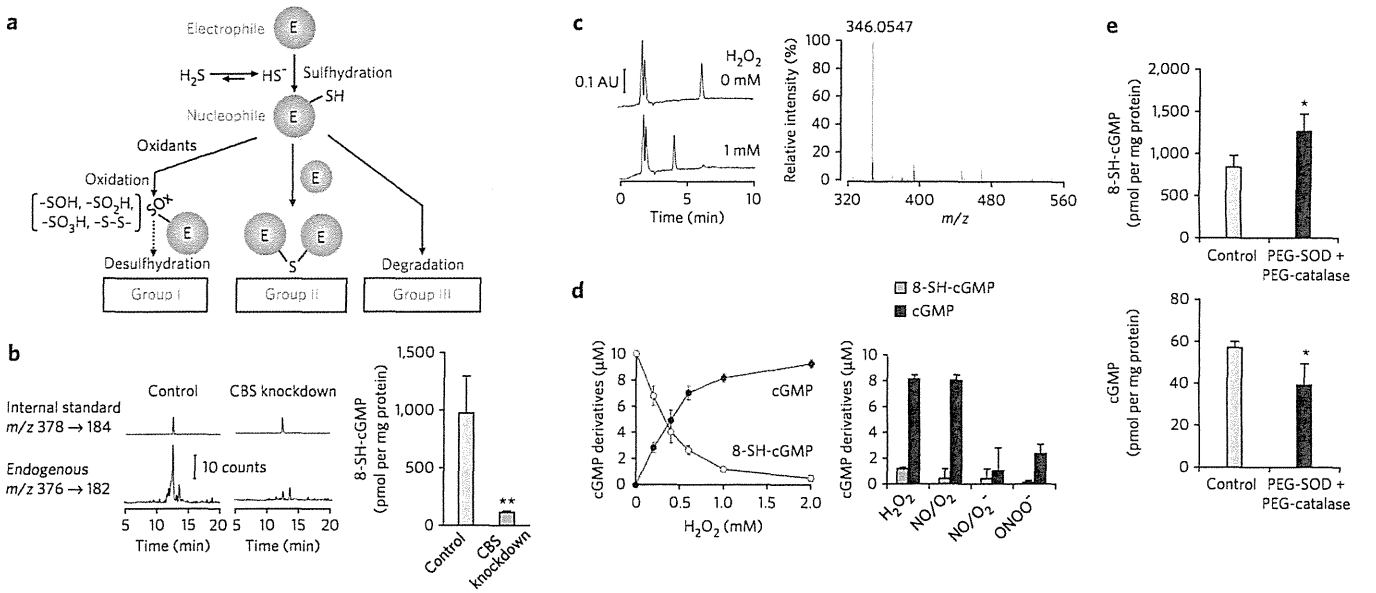

Figure 3 | Cellular formation of 8-SH-cGMP and its metabolic fate. (**a**) Metabolic fate of electrophiles after reaction with HS^-. Details of the classification are shown in **Supplementary Figure 6**. (**b**) Formation of 8-SH-cGMP and its suppression by CBS knockdown in 8-nitro-cGMP-treated A549 cells. 8-SH-cGMP formation was determined via LC-ESI-MS/MS (8-[^{34}SH]-cGMP was used as an internal standard). Data represent mean ± s.d. ($n = 3$). $^{**}P < 0.01$. (**c**) Oxidative desulfhydration of 8-SH-cGMP by H_2O_2 to form cGMP. Left, the reaction of 8-SH-cGMP (10 μM) with H_2O_2 (1 mM) led to the disappearance of 8-SH-cGMP (elution time, 6 min) and appearance of a new peak (elution time, 4 min). Right, LC/MS identified cGMP as a major product in the reaction of 8-SH-cGMP with H_2O_2. AU, arbitrary unit. (**d**) Oxidative desulfhydration of 8-SH-cGMP by H_2O_2 and RNOS. 8-SH-cGMP (10 μM) was reacted with various concentrations of H_2O_2 (left) and with H_2O_2 and RNOS (1 mM each) (right). NO/O_2: NO under aerobic conditions, producing nitrogen oxides; NO/O_2^-: simultaneous generation of NO and O_2^- by 3-morpholinosydnonimine (SIN-1) to form $ONOO^-$ *in situ*; $ONOO^-$: synthetic $ONOO^-$. Data represent mean ± s.d. ($n = 3$). (**e**) Stability of 8-SH-cGMP formed from 8-nitro-cGMP in A549 cells enhanced by antioxidant enzymes. A549 cells were treated with 8-nitro-cGMP (200 μM) in the absence and presence of antioxidant PEG-SOD (100 U ml^{-1}) and PEG-catalase (200 U ml^{-1}) for 6 h. LC-ESI-MS/MS was used to determine 8-SH-cGMP and cGMP formation. Data represent mean ± s.d. ($n = 3$). $^{*}P < 0.05$.

treated with various oxidants, specifically treatment resulting in a rapid oxidative desulfhydration as described below (**Fig. 3**). Certain lipid-derived endogenous electrophiles, such as HNE and acrolein, degraded rapidly after reacting with HS^-, without forming any appreciable products detected by RP-HPLC (**Fig. 2c**). Michael adducts of HNE with cysteine and histidine, HNE-His and HNE-Cys, were resistant to the same HS^- reaction, suggesting that both HNE and acrolein undergo efficient HS^--induced decomposition in a manner dependent on their strong electrophilicity (**Supplementary Fig. 4d**). Consistent with these findings, the Michael adduction of cellular proteins by 1,2-NQ or acrolein was markedly enhanced when CBS was knocked down in A549 cells (**Fig. 2d**). These data support the regulation of not only electrophilic S-guanylation but also S-alkylation or S-arylation of cellular proteins by HS^- reactions with the parent electrophile. The relative reactivities of electrophiles with HS^- was estimated by the rate of consumption of electrophiles in the presence of HS^-. Acrolein showed the highest reactivity with HS^-, with relative reactivities decreasing in the order $OANO_2$ > HNE > 15d-PGJ_2 > 8-nitro-cGMP, whereas the reactivities of these electrophiles with GSH were similar[4,7,8].

Metabolism of sulfhydrated electrophiles and 8-SH-cGMP

The metabolic fate of these sulfhydrated derivatives of electrophiles allowed us to sort the electrophiles into three groups (**Fig. 3a** and **Supplementary Fig. 6**). In group 1, because the SH derivative was so stable, no other reaction occurred except for oxidative modifications of SH by ROS and other reactive species. Group 2 involved relatively stable bis product formation. Group 3 may include other highly reactive electrophiles, such as HNE and acrolein, for which additional metabolism and secondary chemical reactions followed SH addition.

Endogenous HS^--dependent sulfhydration occurred in A549, HepG2 and C6 cells, as evidenced by 8-SH-cGMP formation from exogenously added 8-nitro-cGMP (**Fig. 3b** and **Supplementary Fig. 7**). CBS knockdown markedly inhibited 8-SH-cGMP formation in A549 cells, a finding confirming CBS as a major source of endogenous HS^-. Because 8-SH-cGMP contains sulfhydryls, it is presumably oxygen labile or susceptible to further oxidization. To test this possibility, we treated 8-SH-cGMP with hydrogen peroxide (H_2O_2) and reactive nitrogen oxide species (RNOS) including nitrogen dioxide (NO_2) and peroxynitrite ($ONOO^-$), which stem from the concurrent generation of NO and superoxide (**Fig. 3c,d**). Notably, the sole detectable product of this reaction was cyclic GMP (cGMP) rather than oxidized derivatives of 8-SH-cGMP, such as 8-sulfenyl-, 8-sulfinyl- and 8-sulfonyl-cGMP or 8-OH-cGMP (**Fig. 3c,d**), thus representing what is to our knowledge the first identification of oxidant-induced desulfhydration of SH-containing compounds. Remarkably, the oxidant-labile nature of several sulfhydrated products generated from electrophiles, such as 8-SH-cGMP, 15d-PGJ_2-SH and even sulfhydrated adducts of HNE and acrolein, may reflect their high nucleophilic potential. Thus, secondary redox reactions of nucleophiles derived from HS^--dependent electrophile sulfhydration are expected to affect the biological stability and detection of these sulfhydrated adducts once they are formed in cells. For example, the amounts of 8-SH-cGMP formed in A549 and HepG2 cells were smaller than expected on the basis of the amounts of HS^- produced in the same cells, as assessed by LC-ESI-MS/MS described below (**Figs. 3b** and **4a** and **Supplementary Fig. 7c**); C6 cells, however, did not show the same result (**Supplementary Fig. 7d**). The small amounts of 8-SH-cGMP that were detected compared with the amount of HS^- generated may thus be due to instability induced by the nucleophilicity of 8-SH-cGMP. This view is substantiated by the finding that cell treatment with PEG-derivatized SOD

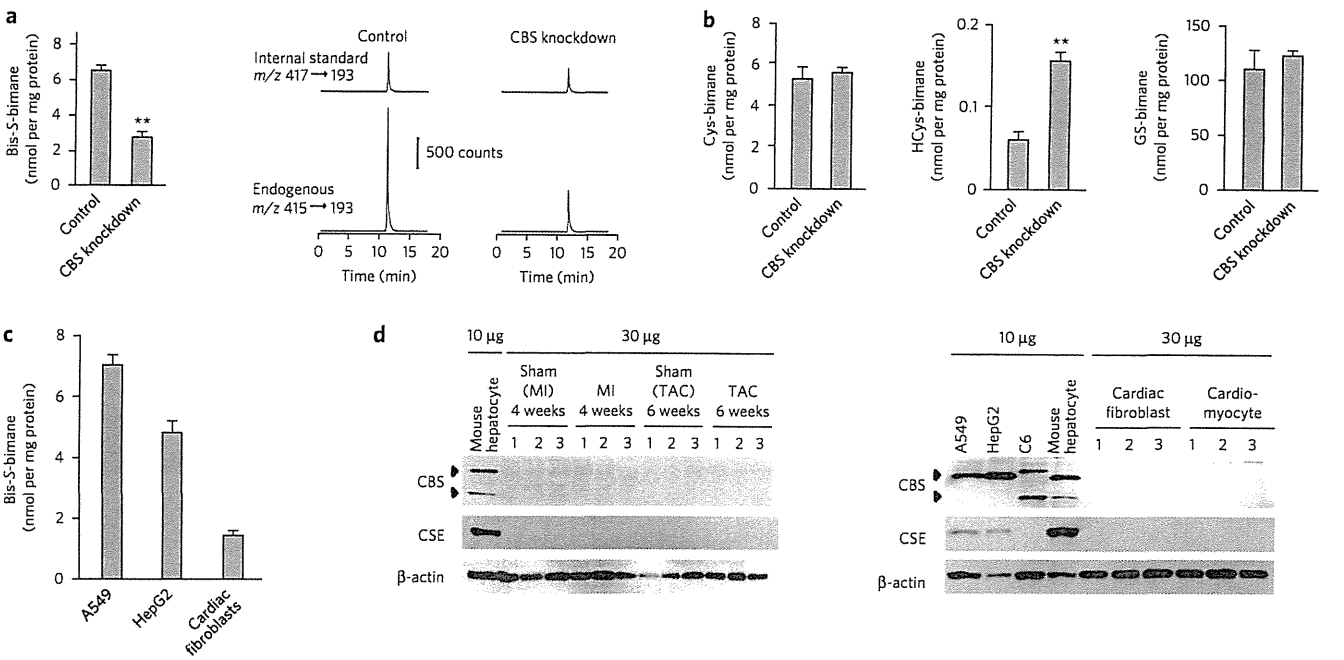

Figure 4 | Cellular HS^- formation and its physiological relevance to electrophile metabolism. (**a**) Quantification by LC-ESI-MS/MS coupled with a monobromobimane-based assay of HS^- formed by A549 cells treated with CBS siRNA or untreated cells. Data represent mean ± s.d. ($n = 3$). $^{**}P < 0.01$. CBS knockdown was confirmed by western blot (**Supplementary Fig. 7b**). (**b**) Quantification of low-molecular-weight thiols in A549 cells with and without CBS knockdown. Data represent mean ± s.d. ($n = 3$). $^{**}P < 0.01$. GS-bimane, glutathione-bimane. (**c**) Comparison of HS^- production in cultured cells. Data represent mean ± s.d. ($n = 3$). (**d**) Western blots for expression of CBS and CSE in various cultured cells and rat cardiac cells. Mouse cardiac tissues were analyzed 4 weeks after sham operation or myocardial infarction or 6 weeks after sham operation or TAC (top). Cultured cells (A549, HepG2, C6, mouse hepatocytes) and rat cardiac fibroblasts and myocytes were analyzed for expression of CBS and CSE. Uncropped blots are shown in **Supplementary Figure 18**.

(PEG-SOD) and catalase (PEG-catalase) significantly improved the recovery of 8-SH-cGMP and simultaneously reduced cGMP formation from 8-nitro-cGMP administered to A549 cells in culture ($P < 0.05$; **Fig. 3e**). Because cGMP, a desulfhydrated product of 8-SH-cGMP, is metabolized by a diversity of cellular phosphodiesterases (PDEs), oxidative desulfhydration by HS^- may also contribute to physiological decomposition of 8-nitro-cGMP.

HS^- formation in cells and myocardial tissues

The electrophilic fluorogenic reagent monobromobimane, typically used to analyze thiols, undergoes HS^--dependent sulfhydration to yield a bis-*S*-bimane derivative[15]. We capitalized on this bimane reaction for sensitive and specific HS^- measurement using LC-ESI-MS/MS (**Supplementary Fig. 7a**) and detected remarkable endogenous HS^- generation in A549 and HepG2 cells and cells in primary culture, specifically rat cardiomyocytes and cardiac fibroblasts (**Fig. 4**). CBS knockdown greatly suppressed the extent of HS^- generation in A549 cells (**Fig. 4a**). Other cell lines, including HepG2 and C6 cells, also showed suppressed HS^- generation after CBS knockdown (**Supplementary Fig. 7c,d**).

A technical advantage of bimane sulfhydration analysis by LC-ESI-MS/MS is the ability to measure in parallel all low-molecular-weight sulfhydryls: not only HS^- but also cysteine, HCys and GSH. For example, the amounts of intracellular cysteine and GSH were not altered by cell treatment with CBS siRNA (**Fig. 4b**). CBS siRNA treatment of cells reduced only amounts of HS^- and instead increased the intracellular level of HCys, a substrate for CBS that accumulated after CBS knockdown (**Fig. 4a,b**), suggesting the critical involvement of HS^- rather than other cysteine-related derivatives in electrophile metabolism, particularly for 8-nitro-cGMP. This suggestion is supported by the fact that the pK_a values of these cysteine-related compounds (8.3, 10.0 and 8.8 for cysteine, HCys and GSH, respectively[16,17]) are much higher than that of H_2S (6.7), which indicates higher nucleophilic reactivity of HS^- compared with other compounds at more physiological pH values, as its nucleophilicity is determined by its low pK_a[18].

Bimane sulfhydration analysis also showed much lower HS^- production in primary cultures of cells (for example, rat cardiomyocytes and cardiac fibroblasts) compared with cultures of all tumor cell lines examined (**Fig. 4c**). Lower CBS and CSE expression in these primary cell cultures was also evident, as compared with that in mouse hepatocytes and tumor cell lines (A549, HepG2 and C6 cells) (**Fig. 4d**). The finding that myocardial cells and tissues produced less HS^- than the other cells studied suggests that the amount of endogenous HS^- in the heart may be limiting in the context of the amounts of endogenous electrophiles that can be generated during both basal metabolism and inflammatory responses. In other words, myocardial cells may be relatively sensitive to endogenous electrophiles, particularly when they are generated excessively during inflammatory processes.

Notably, HS^- is a ubiquitous constituent of many buffers and cell culture media and is not just a product of the cysteine biosynthetic enzymes CBS and CSE[13,19]. For example, fresh DMEM contained an appreciable amount of HS^- (**Supplementary Fig. 7e**). Therefore, HS^- rather than H_2S gas may be widely distributed endogenously, in equilibrium with environmental sources and as a byproduct of the decay of more complex thiols. Because HS^- can act partly as a potent quencher of various electrophiles, even trace amounts of this ubiquitous mediator will affect the detection and actions of endogenously generated electrophiles in biological systems.

Electrophilic H-Ras activation is regulated by HS^-

Recent studies of oxidative inflammatory reactions suggest that an H-Ras oncogenic cellular response can be induced by NO^- or

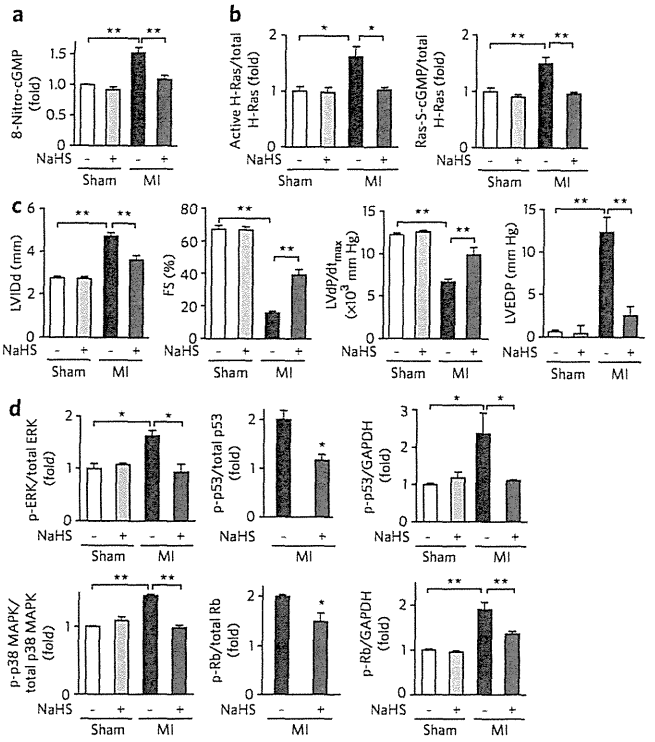

Figure 5 | Electrophilic H-Ras activation regulated by HS^- in cells and *in vivo* in cardiac tissues. (**a**) Immunohistochemical determination of 8-nitro-cGMP formation in mouse hearts after myocardial infarction (MI) after NaHS treatment or in untreated (vehicle) hearts (original images are in **Supplementary Fig. 8d**). Data represent mean ± s.e.m. $^{**}P < 0.01$. (**b**) Quantitative data for western blots of H-Ras activation and S-guanylation in mouse hearts (original blots are in **Supplementary Fig. 8f**). Data represent mean ± s.e.m. $^{*}P < 0.05$, $^{**}P < 0.01$. (**c**) Protective effects of HS^- on chronic heart failure caused by myocardial infarction. Cardiac functions of mice after myocardial infarction or sham operation and treated with NaHS or untreated (treated with vehicle). LVIDd, left ventricular end-diastolic internal diameter; FS, fractional shortening; dP/dt_{max}, maximal rate of pressure development; EDP, end-diastolic pressure. Data represent mean ± s.e.m. $^{**}P < 0.01$. (**d**) Quantitative data for western blots measuring amount of phosphorylation (p-) of ERK, p38 MAPK, p53 and Rb and expression of ERK, p38 MAPK, p53 and Rb in mouse hearts after myocardial infarction (original blots are in **Supplementary Fig. 8f**). Because western blotting detected no expression of Rb and p53 in sham-operated mouse hearts, the amounts of phosphorylation of p53 and Rb were compared after normalization with GAPDH as an internal control. Data represent mean ± s.e.m. $^{*}P < 0.05$, $^{**}P < 0.01$.

RNOS-derived species and the electrophile 15d-PGJ_2 (refs. 20,21), which in turn may activate p53-dependent cellular senescence[22,23]. We examined the effect of exogenously administered or endogenous HS^- in this context, focusing on an electrophilic signaling pathway mediated by H-Ras and p53 that may be activated by 8-nitro-cGMP or other electrophiles formed in cells.

Because less HS^- was produced—that is, endogenous HS^- may have been in short supply relative to the amount of endogenous electrophiles in myocardial cells and tissues (**Fig. 4**)—we evaluated pharmacological activities of HS^- in cardiac cells and in an *in vivo* model of cardiac inflammatory injury. To clarify the physiological functions of HS^-, we induced myocardial hypertrophy and allied chronic inflammatory tissue responses in mouse models of myocardial infarction and pressure overload generated via transverse aortic constriction (TAC) (**Supplementary Fig. 8**). Chronic heart failure after myocardial infarction is a major cause of morbidity and mortality worldwide[24], and both myocardial infarction and TAC models manifest chronic heart failure. Inflammatory reactions that evoke oxidative stress and nitrative stress induced by NO and ROS have been implicated in the genesis of chronic heart failure[25,26], findings supported by our immunohistochemical detection of nitric oxide synthase (NOS)-dependent 8-nitro-cGMP formation in the TAC-induced hypertrophic heart and in non-infarcted heart lesions after myocardial infarction (**Fig. 5a** and **Supplementary Fig. 8a–c**). Substantial 8-nitro-cGMP production, which depended on inducible NOS (iNOS) expression and activity, was strongly inhibited by NaHS treatment of mice after myocardial infarction (**Fig. 5a** and **Supplementary Fig. 8d**). NaHS treatment had no appreciable effects on the tyrosine nitration reaction occurring in cardiac tissues, as assessed by immunohistochemistry and HPLC-based electrochemical detection analysis for 3-nitrotyrosine (**Supplementary Fig. 9a**)[4]. Continuous administration of NaHS to mice after myocardial infarction led to elevated plasma HS^- (4.9 ± 0.4 μM (n = 4; vehicle control) versus 7.1 ± 1.3 μM (n = 7; NaHS-treated)), determined via an LC/MS/MS bimane assay at 4 weeks after myocardial infarction ($P < 0.05$; Student's t-test). Other metabolic pathways related to cGMP biosynthesis and degradation, such as those involving soluble guanylate cyclase and PDEs, were not affected by the same treatment (**Supplementary Fig. 9b,c**). This observation confirms pronounced pharmacological actions of HS^- and subsequent electrophile sulfhydration *in vivo* in cardiac cells and tissues.

We then investigated H-Ras activation in cardiac tissue in which increased iNOS expression and concomitant 8-nitro-cGMP production occurred. Affinity capture analyses were used to detect H-Ras activation in the tissues. Western blotting of proteins involved in myocardial infarction- and TAC-induced chronic heart failure showed H-Ras activation and simultaneous S-guanylation of activated H-Ras pulled down from hypertrophic cardiac tissue (**Fig. 5b** and **Supplementary Fig. 8e**). NaHS treatment also fully inhibited H-Ras activation and concomitant H-Ras S-guanylation in mouse hearts after myocardial infarction (**Fig. 5b** and **Supplementary Fig. 8f**).

NaHS treatment *in vivo* after myocardial infarction greatly improved dilation of the left ventricle and limited its dysfunction in mice, although ischemic scars were equally developed in hearts of both NaHS- and vehicle-treated mice (**Fig. 5c** and **Supplementary Table 2**). A critical downstream cellular response to Ras activation is mediated by ERK, p38 MAPK and phosphatidylinositol-3-kinase (PI3K), which have a central role in cardiac hypertrophy[27]. Sustained activation of ERK and p38 MAPK then induces activation of p53 and Rb, which have a critical function in cellular senescence[22,23] and the transition from hypertrophy to heart failure[28,29]. NaHS treatment strongly suppressed the activation of ERK and p38 MAPK. Furthermore, phosphorylation of p38 MAPK, ERK, p53 and Rb increased in mouse hearts after myocardial infarction, with NaHS suppressing their activation (**Fig. 5d** and **Supplementary Fig. 8g**). These results confirm that HS^- attenuates left ventricle dilation and dysfunction after myocardial infarction, in part by suppressing myocardial cell S-guanylation–dependent activation of H-Ras and its downstream signaling pathways.

We identified high HS^- production (**Fig. 4**) and constitutive expression of different NOS isoforms[30,31] in A549 cells and identified concomitant baseline protein S-guanylation by endogenous 8-nitro-cGMP, as evidenced by western blot analysis (**Fig. 1a,b**). Strong H-Ras activation was induced by CBS knockdown in A549 cells, with simultaneous S-guanylation of activated H-Ras pulled down from the same cell lysates (**Supplementary Fig. 10a**). Such elevated S-guanylation and activation of H-Ras induced by CBS knockdown were completely nullified by addition of NaHS. The same enhancement of H-Ras activation by S-guanylation was observed when 8-nitro-cGMP was added to cultured A549 cells (**Supplementary Fig. 10b**). This observation

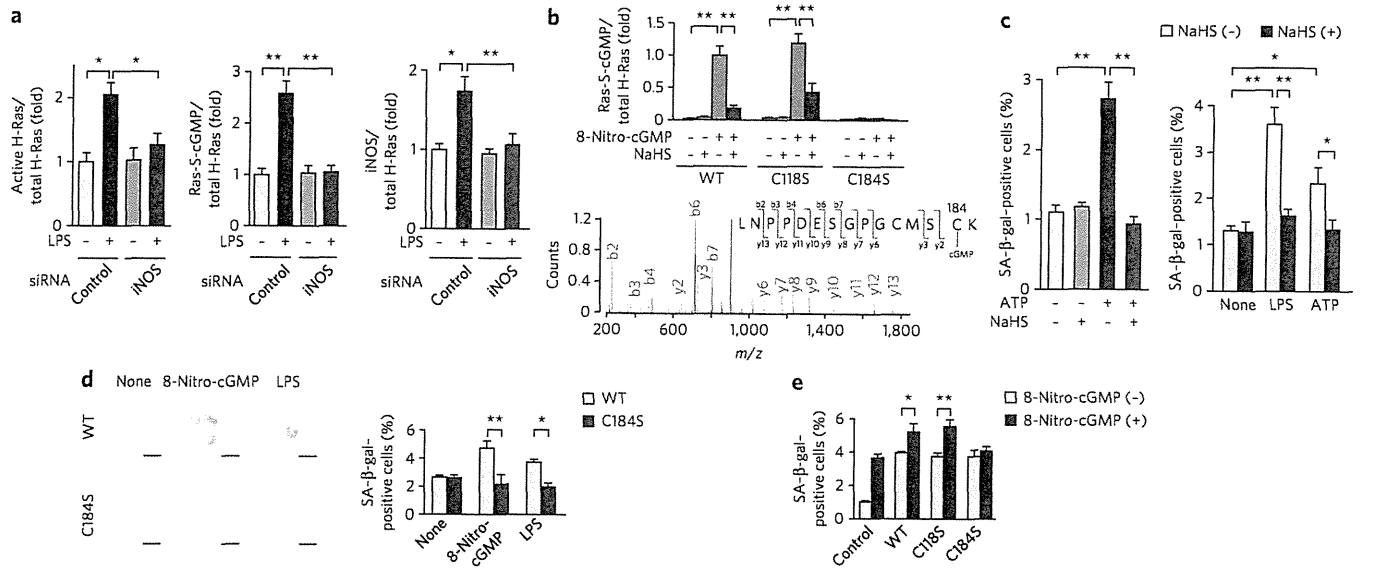

Figure 6 | HS^- regulation of H-Ras electrophile sensing and signaling. (**a**) Suppression of LPS-induced iNOS expression, S-guanylation and activation of H-Ras by iNOS knockdown in rat cardiac fibroblasts in culture. (**b**) Identification of the S-guanylation site in H-Ras. Top, quantitative data for western blotting of S-guanylation in recombinant H-Ras (wild-type (WT) and C118S and C184S mutants) treated with 8-nitro-cGMP (10 μM) and its suppression by NaHS (100 μM). Bottom, MS identification of S-guanylation at Cys184 in recombinant H-Ras treated with 8-nitro-cGMP (10 μM). (**c**) Induction of rat cardiomyocyte senescence by ATP (100 μM) treatment (left) and in cardiac fibroblasts stimulated with LPS and ATP (right) and their suppression by NaHS (100 μM). Cells were stimulated with LPS (1 μg ml^{-1}) or ATP (100 μM) for 3 h, followed by incubation in 0.5% (v/v) serum-containing medium for 4 d. In some experiments, cells were pretreated with 100 μM NaHS for 1 h before stimulation with LPS or ATP. (**d**) Senescence induction of rat cardiac fibroblasts expressing WT or $H\text{-}Ras^{C184S}$ by 8-nitro-cGMP (10 μM) or LPS (1 μg ml^{-1}). Scale bars, 20 μm. (**e**) 8-Nitro-cGMP-induced (10 μM) senescence of rat cardiac fibroblasts transfected with control vector or vectors expressing wild-type H-Ras or $H\text{-}Ras^{C118S}$ or $H\text{-}Ras^{C184S}$ mutants. In **c** and **d**, cell senescence was determined by SA-β-gal staining with quantitative analysis. Data represent mean ± s.e.m. $*P < 0.05$, $**P < 0.01$. Original images for **a**–**c** and **e** are shown in **Supplementary Figure 11**.

confirmed the substantial contribution of elevated endogenous 8-nitro-cGMP, generated by CBS knockdown, to H-Ras activation. Although an involvement of endogenous HNE formation was not evident, marked activation of H-Ras via S-alkyl adduction occurred in HNE-treated A549 cells and was inhibited by CBS-derived HS^- (**Supplementary Fig. 10c**). These data reveal that HS^- can regulate cellular electrophilic signaling involving H-Ras via electrophile sulfhydration reactions.

Electrophilic H-Ras signaling regulated by HS^-

iNOS-dependent H-Ras S-guanylation concomitant with H-Ras activation was confirmed with rat cardiac fibroblasts in culture with or without iNOS knockdown after lipopolysaccharide (LPS) stimulation to generate endogenous 8-nitro-cGMP (**Fig. 6a** and **Supplementary Fig. 11a**). Suppression of iNOS expression by the siRNA resulted in almost complete abrogation of H-Ras S-guanylation and activation in the cardiac fibroblasts. Site-specific

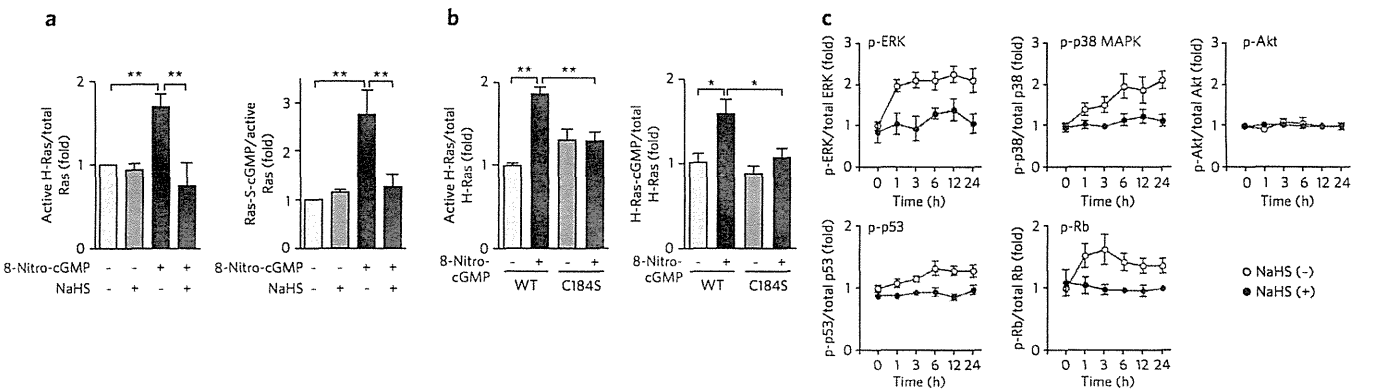

Figure 7 | 8-Nitro-cGMP-induced H-Ras activation in cardiac cells and their suppression by HS^-. (**a**) 8-Nitro-cGMP-induced H-Ras activation with its concomitant S-guanylation in rat cardiomyocytes and their suppression by HS^-. Rat cardiomyocytes were pretreated with NaHS (100 μM) for 24 h, followed by incubation with 8-nitro-cGMP (10 μM) for 4 d. Data represent mean ± s.e.m. $**P < 0.01$. (**b**) 8-Nitro-cGMP-induced activation of H-Ras via S-guanylation at Cys184 in membrane preparation of rat cardiac fibroblasts. Cardiac membranes expressing GFP-fused WT H-Ras or $H\text{-}Ras^{C184S}$ mutants were treated with 8-nitro-cGMP (10 μM) for 1 h. Data represent mean ± s.e.m. $*P < 0.05$, $**P < 0.01$. (**c**) Time courses of phosphorylation (p-) of ERK, p38 MAPK, Akt, p53 and Rb induced by 8-nitro-cGMP (10 μM) in rat cardiomyocytes. Cells were untreated or treated with NaHS (100 μM) 24 h before 8-nitro-cGMP treatment. Data represent mean ± s.e.m. Original western blots for **a**–**c** are shown in **Supplementary Figure 14**.

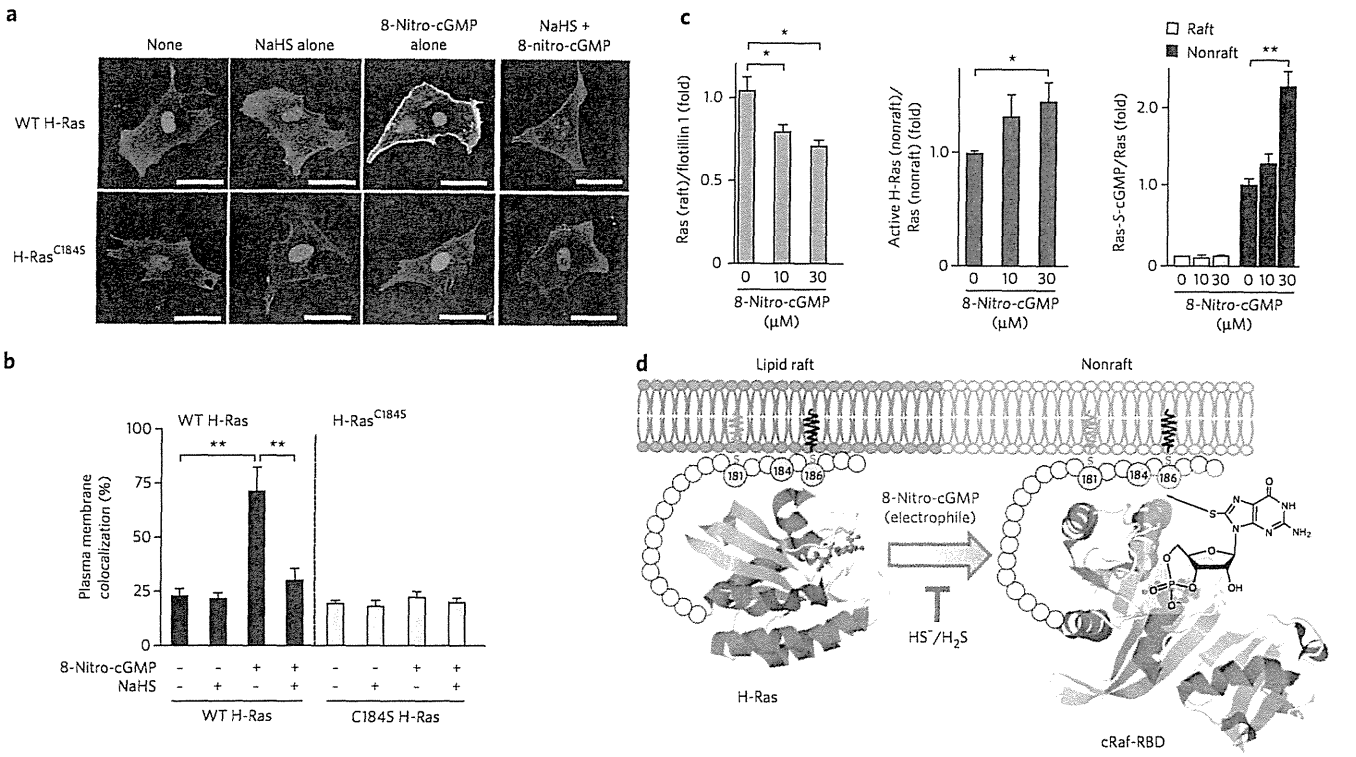

Figure 8 | Dissociation of H-Ras from rafts and its activation induced by H-Ras Cys184 S-guanylation. (**a**) 8-Nitro-cGMP-induced colocalization of H-Ras with the Ras-binding domain (RBD) at the plasma membrane of rat cardiac fibroblasts. Cells expressing GFP-fused H-Ras and DsRed-fused cRaf-RBD proteins were pretreated for 3 h with cycloheximide (50 μg ml^{-1}) and then incubated for 3 h in cycloheximide with or without NaHS (100 μM). Then, cells were untreated or treated with 8-nitro-cGMP (10 μM) for 3 h. Merge images of GFP-fused H-Ras and DsRed-fused cRaf-RBD are shown (individual images of GFP-fused H-Ras, DsRed-fused cRaf-RBD, differential interference contrast (DIC) images are in **Supplementary Fig. 16a,b**). Scale bars, 50 μm. (**b**) Quantitative data obtained from morphometric analysis for colocalization of H-Ras and cRaf-RBD at the plasma membrane shown in **a**. Data represent mean ± s.e.m. $^{**}P < 0.01$. (**c**) 8-Nitro-cGMP-induced H-Ras dissociation from rafts with concomitant S-guanylation and the implication of this dissociation in H-Ras activation. Western blotting of H-Ras, flotillin 1 and S-guanylated H-Ras for the raft fraction and active H-Ras, S-guanylated H-Ras and H-Ras for the nonraft fraction in the presence or absence of 8-nitro-cGMP (uncropped blots are in **Supplementary Fig. 16c**). Data represent mean ± s.e.m. $^{*}P < 0.05$, $^{**}P < 0.01$. (**d**) Schematic model showing activation of H-Ras induced by 8-nitro-cGMP. Gray lipid indicates palmitoylation (at Cys181), and black lipid indicates isoprenylation (at Cys186). The yellow balls are cysteine residues. Magenta ribbons represent α-helices, and yellow ribbons represent β-sheets. T indicates that HS^-/H_2S inhibits the reaction mediated by the electrophile 8-nitro-cGMP. The three-dimensional structures of H-Ras and Raf-RBD were obtained from the Protein Data Bank under accession codes 3L8Z (right) and 3KUD (left).

H-Ras S-guanylation and its inhibition by HS^- were verified in a cell-free reaction mixture via western blotting and proteomic analysis of recombinant H-Ras and its C184S mutant treated with 8-nitro-cGMP (**Fig. 6b** and **Supplementary Fig. 11b**). LC/MS/MS sequencing analysis revealed that only Cys184 of H-Ras was S-guanylated (**Fig. 6b**). Thus, H-Ras Cys184 is a highly susceptible nucleophilic sensor for 8-nitro-cGMP–induced protein S-guanylation.

Oxidative stress–related nucleotides that induce DNA and nucleotide damage and activation of oncogenic Ras can induce cellular senescence via p53 and Rb tumor suppressor pathways[22,23] (**Supplementary Fig. 12**). Thus, we investigated how 8-nitro-cGMP formation may promote cardiac cell senescence. Exogenously administered 8-nitro-cGMP, but not NO or cGMP, caused growth arrest and remarkably increased the senescence of cultured rat cardiac fibroblasts, with NaHS treatment limiting these responses (**Supplementary Fig. 11c,d**). The 8-nitro-cGMP–related senescence responses of the cultured cardiomyocytes were comparable to those of cells expressing Ras^{G12V}, a constitutively active form of Ras (**Supplementary Fig. 11e**). Therefore, the impact of site-specific H-Ras Cys184 S-guanylation was evaluated in the context of downstream signaling reactions leading to cellular senescence of cultured rat cardiac fibroblasts. Enhanced senescence of fibroblasts occurred after 8-nitro-cGMP treatment or after stimulation with LPS to generate endogenous 8-nitro-cGMP (**Fig. 6c–e** and **Supplementary Figs. 11** and **13**). Both LPS and ATP induce iNOS expression and NO synthesis in cardiac cells[32]. Here, ATP addition activated cultured cardiomyocytes to generate 8-nitro-cGMP, the amounts of which corresponded to the degree of protein S-guanylation (**Supplementary Fig. 13a**). This generation of 8-nitro-cGMP induced cellular senescence (**Fig. 6c** and **Supplementary Fig. 11f,g**). NaHS treatment markedly attenuated 8-nitro-cGMP formation and protein S-guanylation, which resulted in suppression of cellular senescence induced by electrophilic stimulation in these cultured rat cardiac cells (**Fig. 6c** and **Supplementary Fig. 13**). The senescence occurred only when cells expressed wild-type H-Ras or the $H\text{-}Ras^{C118S}$ mutant but not the $H\text{-}Ras^{C184S}$ mutant (**Fig. 6d,e** and **Supplementary Fig. 11h**).

Treatment of cultured rat cardiomyocytes with 8-nitro-cGMP also induced H-Ras activation with simultaneous H-Ras S-guanylation, which was strongly inhibited by NaHS treatment (**Fig. 7a** and **Supplementary Fig. 14a**). Moreover, activation of H-Ras, but not of the $H\text{-}Ras^{C184S}$ mutant, was induced in the membrane preparation of rat cardiac fibroblasts after treatment with 8-nitro-cGMP (**Fig. 7b** and **Supplementary Fig. 14b**). Inhibition of ERK, p38 MAPK and PI3K greatly suppressed 8-nitro-cGMP–induced cardiac senescence (**Supplementary Fig. 14c,d**). In contrast, treatment of cardiomyocytes with 8-nitro-cGMP induced sustained activation of ERK, p38 MAPK, p53 and Rb but not of Akt, a downstream effector of

class I PI3K, which was nullified by the NaHS treatment (**Fig. 7c** and **Supplementary Fig. 14e**). We conclude that Cys184 of H-Ras is a functionally critical sensor of endogenous electrophilic species, such as 8-nitro-cGMP, in their H-Ras–dependent downstream signal transduction.

Among Ras isoforms, only H-Ras contains two palmitoylation sites (Cys181 and Cys184), and palmitoylation of Ras proteins has a key role in their localization and activity[33]. Monopalmitoylation of Cys181, but not Cys184, was sufficient to target H-Ras to the plasma membrane, and GDP-bound H-Ras was detected predominantly in lipid rafts (**Supplementary Fig. 12**)[34,35]. GTP loading of H-Ras released H-Ras from the rafts to become more diffusely distributed in the plasma membrane, an event necessary for efficient activation of Raf[34]. Although the GFP-fused H-Ras and the DsRed-fused Ras-binding domain of cRaf (cRaf-RBD) proteins did not colocalize in cardiac fibroblasts, treatment with 8-nitro-cGMP induced association of H-Ras with cRaf-RBD near the plasma membrane (**Fig. 8a,b** and **Supplementary Fig. 16a,b**). Such 8-nitro-cGMP–dependent colocalization of H-Ras and Raf was not observed in the cells transfected with the $H\text{-}Ras^{C184S}$ mutant (**Fig. 8a,b** and **Supplementary Fig. 16a,b**). This observation indicates that 8-nitro-cGMP promotes activation of H-Ras in the plasma membrane. Because Cys184 palmitoylation leads to the correct GTP-regulated lateral segmentation of H-Ras between lipid rafts and nonraft microdomains[33–35], S-guanylation of H-Ras at Cys184 is expected to redistribute H-Ras from rafts into the bulk plasma membrane. Remarkably, application of 8-nitro-cGMP to the lipid raft fraction isolated from adult rat hearts induced dissociation of GDP-bound H-Ras from rafts, and this H-Ras, no longer associated with a raft and concomitantly S-guanylated, preferentially interacted with cRaf-RBD (**Fig. 8c** and **Supplementary Fig. 16c**). The GDP-bound H-Ras without S-guanylation was left in rafts. NaHS treatment completely suppressed 8-nitro-cGMP–induced colocalization of H-Ras with cRaf-RBD and H-Ras dissociation from rafts. These results indicate that S-guanylation of H-Ras at Cys184 releases H-Ras from lipid rafts and that released H-Ras binds Raf, which leads to activation of downstream signaling pathways (**Fig. 8d** and **Supplementary Fig. 12**).

DISCUSSION

This study reveals that enzymatically generated HS^- regulates the metabolism and signaling actions of various electrophiles and that HS^--induced electrophile sulfhydration regulates electrophile-mediated redox signaling. Although H_2S is proposed to have anti-inflammatory and antioxidant effects, NaHS treatment produced no appreciable suppression of iNOS and NADPH oxidase (Nox2) expression and 3-nitrotyrosine formation in a mouse model of ischemic heart injury (**Supplementary Figs. 9a** and **15a**). NaHS treatment also did not affect LPS-induced ROS production and ATP-induced RNOS generation in cardiac cells and C6 cells in culture (**Supplementary Fig. 15b,c**). In view of the modest rate constants for the reaction of H_2S with ROS and RNOS such as H_2O_2 and $ONOO^-$ (ref. 36), HS^- is not expected to directly scavenge oxygen or NO-derived reactive species, unless they have a substantial electrophilic character. Moreover, some potential HS^- targets such as the ATP-sensitive K^+ (K_{ATP}) channels[37] and PDEs[38] may be responsible for cardioprotection observed with HS^- treatment. However, inhibition of K_{ATP} channels, protein kinase A or protein kinase G did not affect NaHS-induced suppression of cardiac cell senescence caused by 8-nitro-cGMP (**Supplementary Fig. 14f,g**). Also, NaHS treatment had no effect on cGMP metabolic pathways *in vivo* and *in vitro* (**Supplementary Fig. 9b,c**). Therefore, an unambiguous cause-and-effect relationship in terms of HS^- regulation of electrophile-evoked cellular stress responses leading to cellular senescence exists. H_2S, behaving as an anion (HS^-) rather than as a gaseous molecule, reacts as a nucleophile to induce the sulfhydration of the electrophile. This results in cardioprotection in a model of heart failure after myocardial infarction by suppressing oxidative stress–induced or electrophile-mediated (for example, by 8-nitro-cGMP) cellular senescence.

Ras proteins have three isoforms, which generate distinct signal outputs despite interacting with a common set of effectors[33]. These biological differences can be accounted for by the 25 C-terminal amino acids of the hypervariable domain, which may contain a protein structure required for Ras to associate with the inner membrane. Cys184 of H-Ras is one of two palmitoylation sites located at its C-terminal domain. Monopalmitoylation of Cys181 is required and sufficient for efficient trafficking of H-Ras to the plasma membrane[35]. Although Cys184 is not essential for targeting H-Ras to the plasma membrane, it is required for control of GTP-regulated lateral segmentation of H-Ras between lipid rafts and nonrafts, which is necessary for efficient activation of Raf[34,35]. In addition, inhibition of Cys184 palmitoylation efficiently delivers H-Ras to the plasma membrane with little Golgi pooling[35], suggesting that S-guanylation of H-Ras at Cys184 promotes H-Ras plasma membrane localization and association with Raf by causing its dissociation from lipid rafts. Cys184 of H-Ras may be chemically modified not only by 8-nitro-cGMP but also by HNE and 15d-PGJ_2, and this H-Ras, thereby modified, may increase interaction with cRaf-RBD (**Supplementary Fig. 16d–g**). Moreover, the electrophilic adduction causes precise structural alterations such that H-Ras is accessible to the effector molecule Raf, which, in turn, readily transduces electrophile-mediated signaling to downstream phosphorylation signaling pathways (**Supplementary Fig. 12**)[22,39]. Although the GTP-bound Ras also bound class I PI3K, S-guanylation of H-Ras never activated Akt (**Fig. 7c**). However, inhibition of PI3K strongly suppressed 8-nitro-cGMP–induced cardiac cell senescence (**Supplementary Fig. 14**), which suggests that another class of PI3K may be involved in H-Ras–mediated cardiac senescence. Electrophile adduction of H-Ras at Cys184 induced cellular senescence through kinase-dependent signaling pathways, and thus Cys184 is a facile redox sensor for any endogenous and exogenous electrophiles and their regulation by endogenous HS^- via sulfhydration (**Supplementary Fig. 12**).

8-SH-cGMP still has cGMP activity, in that it effectively activates PKG (**Supplementary Fig. 9d**). Moreover, it can acquire PDE resistance, which will increase its pharmacological effects as a cGMP analog (**Supplementary Fig. 9e**). Because cGMP itself reportedly has a potent cardioprotective effect, sulfhydration of 8-nitro-cGMP may thus alter its chemical properties so that it can benefit not only chronic heart failure after myocardial infarction but also various other disease processes. Thus, although 8-nitro-cGMP formed in excess in the heart after myocardial infarction may accelerate heart remodeling, HS^- generation in cells and tissues may rectify the pharmacological actions of this electrophilic cGMP analog, for example, by converting the pathological effects of 8-nitro-cGMP into beneficial effects associated with a PDE-resistant cGMP homolog. A similar HS^--mediated bioconversion of an electrophile to a nucleophile would apply to other electrophiles, such as 15d-PGJ_2 (**Fig. 3a**).

p53-dependent G_1 cell cycle arrest aids DNA repair of injured cells to prevent oxidative stress–related genetic mutation and genotoxicity. Abundant GTP in the cellular nucleotide pool seems to be nitrated initially and thus may function as a sensor for nucleotide modification caused by RNOS[12]; this step is believed to be crucial for a cellular oxidative stress response. Also, 8-nitro-GTP becomes an endogenous mutagen when incorporated into DNA[40,41]. Therefore, soluble guanylate cyclase not only contributes to electrophilic 8-nitro-cGMP signaling but also can suppress 8-nitro-GTP and limit mutagenic responses (**Supplementary Fig. 12**). Thus, 8-nitro-cGMP regulation by HS^- limits nitrative modification via sulfhydration, supporting positive genomic and signaling functions and conferring protection against ROS- and RNOS-induced genotoxicity.

In conclusion, our present data reveal an important metabolic relationship between HS^- and oxidative inflammation–derived electrophilic signaling mediators. This identification of HS^--induced electrophile sulfhydration as a mechanism for terminating electrophile-mediated signaling provides a fundamental new way of understanding the regulation of redox cellular signaling and therapeutic strategies for inflammation-related diseases.

METHODS

RNAi screening. To clarify factors contributing to regulation of 8-nitro-cGMP signaling, we performed RNAi screening, as described in **Supplementary Methods**. Detailed protocols and siRNAs used are described in **Supplementary Methods** and **Supplementary Table 1**.

Reaction of electrophiles with HS^- *in vitro*. 8-Nitro-cGMP (100 μM) was reacted with various concentrations of NaHS (the HS^- donor) in 100 mM sodium phosphate buffer (pH 7.4) containing 100 μM diethylenetriaminepentaacetic acid (DTPA) at 37 °C for 5 h. The reaction of 8-nitro-cGMP (100 μM) with NaHS (1 mM) was also carried out in the absence or presence of additives including cysteine (100 μM), metals (150 μM) and metal-containing compounds and proteins (10 μM). Reaction products of 8-nitro-cGMP with NaHS in the absence or presence of additives were analyzed by using RP-HPLC and LC/MS as described in **Supplementary Methods**. 15d-PGJ_2 (1–10 μM) was reacted with NaHS (0–1,000 μM) in 100 mM phosphate buffer (pH 7.4) at 37 °C for 2 h. The reactions of 1,2-NQ (100 μM), 1,4-NQ (100 μM), *tert*-butylbenzoquinone (100 μM) or $OANO_2$ (100 μM) with NaHS (50–800 μM) were carried out in 200 mM potassium phosphate buffer (pH 7.5) at 25 °C for 1 h.

Determination and quantitation of cellular 8-SH-cGMP formation. A549, HepG2 and C6 cells treated with CBS siRNA or untreated cells were incubated with 8-nitro-cGMP (200 μM) in serum-free DMEM at 37 °C for 6 h. 8-SH-cGMP that formed in those cultures was quantified by means of LC-ESI-MS/MS with the use of 8-[^{34}SH]-cGMP as an internal standard. Details are in **Supplementary Methods**.

Measurement of cellular production of HS^- and intracellular thiol derivatives. Cellular production of HS^- was quantified by means of LC-ESI-MS/MS with monobromobimane derivatization. This protocol allowed us to simultaneously quantify HS^- and other low-molecular-weight thiols including cysteine, HCys and GSH, as described in **Supplementary Methods**.

Animals and surgery. All protocols using mice and rats were approved by the Animal Care and Use Committee, Kyushu University. Mice with a homozygous deletion of the gene encoding iNOS were purchased from Jackson Laboratory. The left anterior descending coronary artery (LAD) was ligated (with 6-0 silk suture) near its origin between the pulmonary outflow tract and the edge of the left atrium. Acute myocardial ischemia was deemed successful when the anterior left ventricle wall became cyanotic and the electrocardiogram showed obvious ST segment elevation. Sham-operated mice were subjected to the same procedure, except that the suture around the LAD was not tied. TAC surgery was performed on 6-week-old male C57BL/6J mice. A mini-osmotic pump (Alzet) filled with vehicle (PBS) or NaHS (50 μmol kg^{-1} d^{-1}) was implanted intraperitoneally into 8-week-old male C57BL/6J mice 1 d after LAD ligation. Plasma concentrations of HS^- were determined by means of LC-ESI-MS/MS with monobromobimane as described in **Supplementary Methods**.

Immunological measurement of 8-nitro-cGMP production *in vivo*. Paraffin-embedded left ventricle sections (5 μm thick) were stained with 8-nitro-cGMP (1G6)–specific antibody (1:1,000), followed by visualization with Alexa Fluor 488 rabbit-specific IgG (clone no. A11008) and Alexa Fluor 546 mouse-specific IgG (clone no. A11003) antibodies (1:1,000; Invitrogen). Digital photographs were taken at 600× magnification with a confocal microscope (FV10i, Olympus).

Purification of H-Ras. Recombinant human H-Ras was prepared and purified as described in **Supplementary Methods**.

Pulldown assay and western blotting. Endogenous active H-Ras was obtained by incubating supernatants with glutathione S-transferase–fused cRaf-RBD in the presence of GSH-Sepharose beads, followed by western blotting as described in **Supplementary Methods**.

Identification of S-guanylation sites in H-Ras. S-Guanylation sites were identified by means of MS with trypsin-digested peptide fragments of H-Ras. Details are in **Supplementary Methods**.

Isolation of cardiac cells and measurement of cell senescence. Cardiomyocytes and cardiac fibroblasts were prepared from ventricles of 1- to 2-d-old Sprague-Dawley rats. Cardiac fibroblasts were transfected with control vector or vectors expressing H-Ras (wild-type or carrying the C118S or C184S mutation) via electroporation (1,100 V, 10 ms × 4; NeonTM Transfection System, Life Technologies Corporation). Cardiomyocytes were infected with recombinant adenoviruses expressing LacZ control or Ras^{G12V} at 100 multiplicity of infection 1 h after serum starvation. Twenty-four hours later, cells were pretreated with NaHS (100 μM) for 24 h and then were treated with ATP (100 μM), LPS (1 μg ml^{-1}) or 8-nitro-cGMP (10 μM) for 3 h, after which they were cultured for 4 d in 0.5% (v/v) serum-containing medium. Cardiac cells plated on 35-mm glass-bottom dishes were fixed with 4% (w/v) paraformaldehyde neutral buffer solution, and cellular senescence was assessed by measuring endogenous β-galactosidase (β-gal) activity using a senescence-associated β-gal (SA-β-gal) staining kit (Cell Signaling). Digital photographs were taken at 200× magnification with a Biozero microscope (BZ-8000; Keyence), and the number of β-gal–positive cells ($n > 100$ cells) was calculated by using the BZ-II Analyzer (Keyence), with colorimetric intensity adjusted as the percentage of basal senescent cells approached 1.

Transthoracic echocardiography and cardiac catheterization. Echocardiography was performed in anesthetized mice (50 mg per kg body weight pentobarbital sodium) via the Nemio XG echocardiograph (Toshiba) equipped with a 14-MHz transducer. A 1.4-French micronanometer catheter (Millar Instruments) was inserted into the left carotid artery and advanced retrograde into the left ventricle. Hemodynamic measurements were recorded when the heart rate was stabilized within 500 ± 10 beats per min.

Statistical analysis. Results are presented as mean ± s.e.m. of at least three independent experiments unless specified. Statistical comparisons were made with two-tailed Student's *t*-test or one-way analysis of variance followed by the Student-Newman-Keuls procedure, with significance set at $P < 0.05$.

Other methods. Detailed information is available in the **Supplementary Methods**.

Received 8 February 2012; accepted 4 June 2012; published online 1 July 2012

References

1. Kajimura, M., Fukuda, R., Bateman, R.M., Yamamoto, T. & Suematsu, M. Interactions of multiple gas-transducing systems: hallmarks and uncertainties of CO, NO, and H_2S gas biology. *Antioxid. Redox Signal.* **13**, 157–192 (2010).
2. Li, L., Rose, P. & Moore, P.K. Hydrogen sulfide and cell signaling. *Annu. Rev. Pharmacol. Toxicol.* **51**, 169–187 (2011).
3. Fridovich, I. The biology of oxygen radicals. *Science* **201**, 875–880 (1978).
4. Sawa, T. *et al.* Protein S-guanylation by the biological signal 8-nitroguanosine 3′,5′-cyclic monophosphate. *Nat. Chem. Biol.* **3**, 727–735 (2007).
5. Rhee, S.G. Cell signaling. H_2O_2, a necessary evil for cell signaling. *Science* **312**, 1882–1883 (2006).
6. D'Autréaux, B. & Toledano, M.B. ROS as signalling molecules: mechanisms that generate specificity in ROS homeostasis. *Nat. Rev. Mol. Cell Biol.* **8**, 813–824 (2007).
7. Akaike, T., Fujii, S., Sawa, T. & Ihara, H. Cell signaling mediated by nitrated cyclic guanine nucleotide. *Nitric Oxide* **23**, 166–174 (2010).
8. Rudolph, T.K. & Freeman, B.A. Transduction of redox signaling by electrophile-protein reactions. *Sci. Signal.* **2**, re7 (2009).
9. Forman, H.J., Fukuto, J.M. & Torres, M. Redox signaling: thiol chemistry defines which reactive oxygen and nitrogen species can act as second messengers. *Am. J. Physiol. Cell Physiol.* **287**, C246–C256 (2004).
10. Zaki, M.H. *et al.* Cytoprotective function of heme oxygenase 1 induced by a nitrated cyclic nucleotide formed during murine salmonellosis. *J. Immunol.* **182**, 3746–3756 (2009).
11. Uchida, K. & Shibata, T. 15-Deoxy-$\Delta^{12,14}$-prostaglandin J_2: an electrophilic trigger of cellular responses. *Chem. Res. Toxicol.* **21**, 138–144 (2008).
12. Fujii, S. *et al.* The critical role of nitric oxide signaling, via protein S-guanylation and nitrated cyclic GMP, in the antioxidant adaptive response. *J. Biol. Chem.* **285**, 23970–23984 (2010).
13. Hughes, M.N., Centelles, M.N. & Moore, K.P. Making and working with hydrogen sulfide: the chemistry and generation of hydrogen sulfide *in vitro* and its measurement *in vivo*: a review. *Free Radic. Biol. Med.* **47**, 1346–1353 (2009).
14. Tiranti, V. *et al.* Loss of ETHE1, a mitochondrial dioxygenase, causes fatal sulfide toxicity in ethylmalonic encephalopathy. *Nat. Med.* **15**, 200–205 (2009).
15. Wintner, E.A. *et al.* A monobromobimane-based assay to measure the pharmacokinetic profile of reactive sulphide species in blood. *Br. J. Pharmacol.* **160**, 941–957 (2010).
16. Winterbourn, C.C. & Metodiewa, D. Reactivity of biologically important thiol compounds with superoxide and hydrogen peroxide. *Free Radic. Biol. Med.* **27**, 322–328 (1999).
17. Glushchenko, A.V. & Jocobsen, D.W. Molecular targeting of proteins by L-homocysteine: mechanistic implications for vascular disease. *Antioxid. Redox Signal.* **9**, 1883–1898 (2007).

18. LoPachin, R.M., Gavin, T., Geohagen, B.C. & Das, S. Neurotoxic mechanisms of electrophilic type-2 alkenes: soft-soft interactions described by quantum mechanical parameters. *Toxicol. Sci.* **98**, 561–570 (2007).
19. Ishii, I. *et al.* Murine cystathionine γ-lyase: complete cDNA and genomic sequences, promoter activity, tissue distribution and developmental expression. *Biochem. J.* **381**, 113–123 (2004).
20. Lander, H.M. *et al.* Redox regulation of cell signalling. *Nature* **381**, 380–381 (1996).
21. Oliva, J.L. *et al.* The cyclopentenone 15-deoxy-$\Delta^{12,14}$-prostaglandin J_2 binds to and activates H-Ras. *Proc. Natl. Acad. Sci. USA* **100**, 4772–4777 (2003).
22. Serrano, M., Lin, A.W., McCurrach, M.E., Beach, D. & Lowe, S.W. Oncogenic *ras* provokes premature cell senescence associated with accumulation of p53 and $p16^{INK4a}$. *Cell* **88**, 593–602 (1997).
23. Wu, C., Miloslavskaya, I., Demontis, S., Maestro, R. & Galaktionov, K. Regulation of cellular response to oncogenic and oxidative stress by *Seladin-1*. *Nature* **432**, 640–645 (2004).
24. Shih, H., Lee, B., Lee, R.J. & Boyle, A.J. The aging heart and post-infarction left ventricular remodeling. *J. Am. Coll. Cardiol.* **57**, 9–17 (2011).
25. Liu, Y.H. *et al.* Role of inducible nitric oxide synthase in cardiac function and remodeling in mice with heart failure due to myocardial infarction. *Am. J. Physiol. Heart Circ. Physiol.* **289**, H2616–H2623 (2005).
26. Zhang, P. *et al.* Inducible nitric oxide synthase deficiency protects the heart from systolic overload-induced ventricular hypertrophy and congestive heart failure. *Circ. Res.* **100**, 1089–1098 (2007).
27. Gelb, B.D. & Tartaglia, M. Ras signaling pathway mutations and hypertrophic cardiomyopathy: getting into and out of the thick of it. *J. Clin. Invest.* **121**, 844–847 (2011).
28. Sano, M. *et al.* p53-induced inhibition of Hif-1 causes cardiac dysfunction during pressure overload. *Nature* **446**, 444–448 (2007).
29. Hunter, J.J., Tanaka, N., Rockman, H.A., Ross, J. Jr. & Chien, K.R. Ventricular expression of a MLC-2v-*ras* fusion gene induces cardiac hypertrophy and selective diastolic dysfunction in transgenic mice. *J. Biol. Chem.* **270**, 23173–23178 (1995).
30. Asano, K. *et al.* Constitutive and inducible nitric oxide synthase gene expression, regulation, and activity in human lung epithelial cells. *Proc. Natl. Acad. Sci. USA* **91**, 10089–10093 (1994).
31. Pechkovsky, D.V. *et al.* Pattern of NOS2 and NOS3 mRNA expression in human A549 cells and primary cultured AEC II. *Am. J. Physiol. Lung Cell Mol. Physiol.* **282**, L684–L692 (2002).
32. Nishida, M. *et al.* Heterologous down-regulation of angiotensin type 1 receptors by purinergic P2Y2 receptor stimulation through S-nitrosylation of NF-κB. *Proc. Natl. Acad. Sci. USA* **108**, 6662–6667 (2011).
33. Hancock, J.F. Ras proteins: different signals from different locations. *Nat. Rev. Mol. Cell Biol.* **4**, 373–384 (2003).
34. Prior, I.A. *et al.* GTP-dependent segregation of H-Ras from lipid rafts is required for biological activity. *Nat. Cell Biol.* **3**, 368–375 (2001).
35. Roy, S. *et al.* Individual palmitoyl residues serve distinct roles in H-Ras trafficking, microlocalization, and signaling. *Mol. Cell. Biol.* **25**, 6722–6733 (2005).
36. Carballal, S. *et al.* Reactivity of hydrogen sulfide with peroxynitrite and other oxidants of biological interest. *Free Radic. Biol. Med.* **50**, 196–205 (2011).
37. Zhao, W., Zhang, J., Lu, Y. & Wang, R. The vasorelaxant effect of H_2S as a novel endogenous gaseous K_{ATP} channel opener. *EMBO J.* **20**, 6008–6016 (2001).
38. Bucci, M. *et al.* Hydrogen sulfide is an endogenous inhibitor of phosphodiesterase activity. *Arterioscler. Thromb. Vasc. Biol.* **30**, 1998–2004 (2010).
39. Sun, P. *et al.* PRAK is essential for *ras*-induced senescence and tumor suppression. *Cell* **128**, 295–308 (2007).
40. Yoshitake, J. *et al.* Nitric oxide as an endogenous mutagen for Sendai virus without antiviral activity. *J. Virol.* **78**, 8709–8719 (2004).
41. Ohshima, H., Sawa, T. & Akaike, T. 8-Nitroguanine, a product of nitrative DNA damage caused by reactive nitrogen species: formation, occurrence, and implications in inflammation and carcinogenesis. *Antioxid. Redox Signal.* **8**, 1033–1045 (2006).

Acknowledgments

We thank J.B. Gandy for her editing of the manuscript. Thanks are also due to T. Okamoto, S. Fujii, Md. M. Rahaman, S. Khan, K.A. Ahmed, J. Yoshitake, T. Matsunaga, M.H.A. Rahman, J. Sakamoto, J. Minkyung, K. Hara, M. Goto, F. Sohma, K. Taguchi, T. Miura, T. Toyama, Y. Shinkai, I. Ishii and M. Toyataka for technical assistance; S. Kasamatsu, T. Ida and K. Kunieda for 8-nitro-cGMP preparation; Y. Kawai for technical assistance with LC/MS/MS experiments; H. Arimoto for helpful discussion; and J. Wu for reading our paper to evaluate its concepts and interdisciplinary accessibility. This work was supported in part by Grants-in-Aid for Scientific Research and Grants-in-Aid for Scientific Research on Innovative Areas (Research in a Proposed Area) from the Ministry of Education, Sciences, Sports and Technology, Japan; a grant from the Japan Science and Technology Agency PRESTO program; grants from the Ministry of Health, Labor and Welfare of Japan; and grants from the US National Institutes of Health.

Author contributions

M.N., T.A. and T. Sawa designed the experiment, performed analysis and wrote the paper; N.K., H. Inoue and T. Shibata performed MS analysis, cell biology and mouse and rat studies; K.O., H. Ihara, H.M., H.K., M.S. and M.Y. performed data analyses; B.A.F., A.v.d.V., K.U. and Y.K. designed the experiment and edited the paper.

Competing financial interests

The authors declare competing financial interests: details accompany the online version of the paper.

Additional information

Supplementary information is available in the online version of the paper. Reprints and permissions information is available online at http://www.nature.com/reprints/index.html. Correspondence and requests for materials should be addressed to T.A.

RESEARCH ARTICLE

S-Guanylation of Human Serum Albumin is a Unique Posttranslational Modification and Results in a Novel Class of Antibacterial Agents

YU ISHIMA,[1,2] HITOMI HOSHINO,[1] TAKUYA SHINAGAWA,[1] KAORI WATANABE,[1] TAKAAKI AKAIKE,[3] TOMOHIRO SAWA,[3] ULRICH KRAGH-HANSEN,[4] TOSHIYA KAI,[1,5] HIROSHI WATANABE,[1,2] TORU MARUYAMA,[1,2] MASAKI OTAGIRI[1,6,7]

[1]Department of Biopharmaceutics, Graduate School of Pharmaceutical Sciences, Kumamoto University, Kumamoto 862-0973, Japan

[2]Center for Clinical Pharmaceutical Science, Kumamoto University, Kumamoto, Japan

[3]Department of Microbiology, Graduate School of Medical Sciences, Kumamoto University, Kumamoto 860-0811, Japan

[4]Department of Medical Biochemistry, University of Aarhus, DK-8000 Aarhus C, Denmark

[5]Tohoku Nipro Pharmaceutical Corporation, Fukushima 969-0401, Japan

[6]Faculty of Pharmaceutical Sciences, Sojo University, Kumamoto 860-0082, Japan

[7]DDS Research Institute, Sojo University, Kumamoto 860-0082, Japan

Received 24 January 2012; revised 8 March 2012; accepted 16 March 2012

Published online in Wiley Online Library (wileyonlinelibrary.com). DOI 10.1002/jps.23143

ABSTRACT: 8-Nitroguanosine 3′,5′-cyclic monophosphate (8-nitro-cGMP) is a nitric oxide metabolite and an important second messenger. 8-Nitro-cGMP reacts with sulfhydryl groups forming a novel posttranslational modification, namely, *S*-guanylation. In this work, we found, by using a quantitative competition enzyme-linked immunosorbent assay procedure, that *S*-guanylated human serum albumin (*S*-cGMP-HSA) is a component of normal plasma, and that hemodialysis patients decrease its concentration, on an average, from 68 to 34 nM. End-stage renal disease is often accompanied by septicemia, and we found that *S*-cGMP-HSA possesses an *in vitro* antibacterial effect with half maximal inhibitory concentration of approximately 2 μM against *Escherichia coli* American Type Culture Collection. Our findings indicate that *S*-cGMP-HSA can be regarded as an endogenous antibacterial agent in healthy conditions and as a useful new class of antibacterial agents with a circulation time sufficient for *in vivo* biological activity. The clinical development of *S*-cGMP-HSA as a safe and strong antibacterial agent arisen from endogenous posttranslational modification would be expected. © 2012 Wiley Periodicals, Inc. and the American Pharmacists Association J Pharm Sci

Keywords: Albumin; Drug design; Biomaterials; Oxidation; Nanoparticles; nitric oxide; cysteine; posttranslational modification; antibacterial activity; ligand binding

INTRODUCTION

Posttranslational modifications are essential in their functional regulation. Among these, changes of the redox state of cysteine residues are of great importance. For example, the sulfhydryl moiety can interact with nitric oxide (NO) and thereby form *S*-nitrosothiols (RS-NO).[1–3] RS-NOs may function as NO reservoirs and preserve the antioxidant and other activities of NO.[4,5] Thus, it has been reported that *S*-nitroso human serum albumin (SNO-HSA) may serve *in vivo* as a circulating reservoir for NO produced by the endothelial cells.[6]

Recently, we have discovered that a novel nitrated cyclic nucleotide, namely, 8-nitroguanosine 3′,5′-cyclic monophosphate (8-nitro-cGMP), is generated in a NO-dependent manner.[7] 8-Nitro-cGMP exhibits the strongest redox activity among the nitrated guanine derivatives examined; this activity is different from that activating cGMP-dependent

Correspondence to: Masaki Otagiri (Telephone: +81-96-326-3887; Fax: +81-96-326-5048; E-mail: otagirim@gpo.kumamoto-u.ac.jp); Toru Maruyama (Telephone: +81-96-371-4150; Fax: +81-96-362-7690; E-mail: tomaru@gpo.kumamoto-u.ac.jp)

Journal of Pharmaceutical Sciences

protein kinases.[7] Because 8-nitro-cGMP possesses an electrophilic property, this metabolite can react with sulfhydryl groups of cysteine residues and form a protein-*S*-cGMP adduct, via a novel posttranslational modification, namely, protein *S*-guanylation.[7] Importantly, it has been observed that 8-nitro-cGMP causes *S*-guanylation of Kelch-like erythroid-cell-derived protein with CNC homology-associated protein 1 in C6 glioma cells, which leads to Nrf2 activation and subsequent induction of antioxidant enzymes; thus, 8-nitro-cGMP protects cells against the cytotoxic effects of oxidative stress.[8] Another finding of relevance in this connection was reported by Sawa et al.[9] that 8-nitroguanine and 8-nitroxanthine are present in human urine, the median urinary level of 8-nitroguanine was significantly higher in smokers than in nonsmokers, suggesting that these nitro-derived adducts are present in the human circulation. On the basis of these findings,[7–9] we have focused on *S*-guanylation of components such as albumin in human plasma during chronic inflammatory diseases such as chronic renal failure.

Human serum albumin is a single, nonglycosylated polypeptide that organizes to form a heart-shaped protein with approximately 67% α-helix but no β-sheet.[10] All but one (Cys-34) of the 35 cysteine residues are involved in the formation of stabilizing disulfide bonds. In the circulation, normally about half of the Cys-34 residues are freely accessible, that is, not oxidized or involved in ligand binding, and they represent the largest fraction of free thiols in blood. Therefore, we examined *S*-guanylation of HSA by quantitative competitive enzyme-linked immunosorbent assay (ELISA) using a monoclonal anti-*S*-guanylated protein (8-RS-cGMP) antibody.

In this paper, we studied the presence of *S*-guanylated HSA (*S*-cGMP-HSA) in human plasma of healthy volunteers and hemodialysis (HD) patients. In addition, we examined a biological activity of *S*-cGMP-HSA *in vitro*.

MATERIALS AND METHODS

Materials

Nondefatted HSA (96% pure) was donated by the Chemo-Sera-Therapeutic Research Institute (Kumamoto, Japan), and it was defatted by treatment with charcoal, as described by Chen.[11] Sephadex G-25 (ϕ 1.6 × 2.5 cm^2), Blue Sepharose CL-6B (ϕ 2.5 × 20 cm^2), and RESOURCE PHE columns (ϕ 0.64 × 3 cm^2) were from GE Healthcare (Tokyo, Japan). 1,4-Dithiothreitol (DTT), L-cysteine, and glutathione were purchased from Sigma–Aldrich (St. Louis, Missouri. Sulfanilamide, naphthylethylenediamine-hydrochloride, $HgCl_2$, and $NaNO_2$ were obtained from Nakalai Tesque (Kyoto, Japan). *S*-Nitrosoglutathione (GS-NO) and diethylenetriaminepentaacetic acid (DTPA) were obtained from Dojindo Laboratories (Kumamoto, Japan). Other chemicals were of the best grades commercially available, and all solutions were made in deionized and distilled water.

Blood Samples

Twelve stable HD patients (five men, seven women) aged 25 to 87 years, with a dialysis age ranging between 1 and 9 years, were enrolled in this study. Eleven age- and gender-matched healthy subjects were also investigated as a control group. End-stage renal failure was caused by glomerulonephritis ($N = 5$), nephrosclerosis ($N = 1$), diabetic nephropathy ($N = 5$), and unknown causes ($N = 1$). Blood was collected using a vacuum tube collection system, using heparin as an anticoagulant. Plasma fractions were isolated by centrifugation at 4°C for 20 min (2000*g*), and were immediately frozen in liquid nitrogen prior to long-term storage at −80°C. Studies involving human blood were approved by the Ethics Review Committee for Human Experimentation of our institution, and informed consent was obtained from all subjects.

Modifications of Cys-34 on HSA

First, HSA was treated with DTT, as previously reported.[12] For SNO-HSA, 300 μM DTT-treated HSA was incubated with 3 mM GS-NO for 1 h at 37°C, as previously described.[12] For cysteinyl-HSA (Cys-HSA), 300 μM DTT-treated HSA was incubated with 3 mM L-cysteine for 12 h at 37°C. For *S*-cGMP-HSA, 50 μM DTT-treated HSA was incubated with 500 μM NO_2-cGMP for 5 days at 37°C. After each reaction, the mixtures were applied to a Sephadex G-25 column and eluted with phosphate buffered saline (PBS) to remove unreacted GS-NO, L-cysteine, or NO_2-cGMP, respectively. Then, the modified HSAs were concentrated by ultrafiltration. The protein content of all HSA preparations used in this study was determined by the BCA assay.

Western Blot

We performed Western blotting analysis to assess expression levels of various proteins in cells. Anti-8-RS-cGMP antibody was prepared as described earlier.[7] Immunoreactive bands were detected by using a chemiluminescence reagent (ECL Plus; GE Healthcare, Hino, Japan) with a luminescent image analyzer (LAS1000UV mini; Fuji Photo Film Company, Tokyo, Japan).

Competitive ELISA

To determine the endogenous *S*-cGMP adducts in plasma samples from healthy volunteers and HD patients, we used competitive ELISA as described previously.[7] Briefly, each well of a 96-well microtiter plate was coated with 100 μL of the 8-RS-cGMP-BSA

conjugate (0.5 μg/mL) in PBS, blocked with 0.5% gelatin, and washed three times with PBS containing 0.05% Tween 20 (washing buffer). Wells were incubated at room temperature for 1 h with 0.1 mL of antibodies (0.1 μg/mL) in the presence or absence of plasma samples dissolved in washing buffer. The wells were then washed with washing buffer three times and reacted with horseradish-peroxidase-conjugated antimouse IgG antibody, followed by reaction with *o*-phenylenediamine dihydrochloride.[7] The reaction was terminated by the addition of 0.05 mL of 2.0 M sulfuric acid, and absorbance at 490 nm was read by using a micro-ELISA plate reader.

Circular Dichroism

Circular dichroism (CD) spectra of HSA, SNO-HSA, and *S*-cGMP-HSA were measured at 25°C using a J-720-type spectropolarimeter (JASCO, Tokyo, Japan).[13] For the calculation of mean residue ellipticity [θ], the molecular weight of the albumins was taken as 66,500 Da. Far-UV and near-UV CD spectra were recorded at protein concentrations of 5 and 15 μM, respectively, in 20 mM sodium phosphate buffer (pH 7.4).

Tryptophan Fluorescence

Intrinsic fluorescence spectra of HSA, SNO-HSA, and *S*-cGMP-HSA were measured at a protein concentration of 2 μM and 25°C using a JASCO FP-777 spectrofluorometer equipped with thermostatically controlled 1 cm quartz cells and 5 nm excitation and emission bandwidths. HSA, SNO-HSA, and *S*-cGMP-HSA were excited at 295 nm, and the spectra were corrected for buffer baseline fluorescence.

NO_2^- Measurement

We quantified NO_2^- released from 8-nitro-cGMP during denitration by means of a high-performance liquid chromatography (HPLC) flow reactor system, as reported previously.[14] 8-Nitro-cGMP (0–500 μM) was incubated with 50 μM HSA in 100 mM sodium phosphate buffer (pH 7.4) for 0, 3, 6, 12, 24, 30, 70, 115, or 130 h at 37°C. The reaction solutions were applied to a reverse-phase HPLC column (4.6 × 30 mm^2, CA-ODS; Eicom Company, Kyoto, Japan) to remove the protein in the solutions. NO_2^- was eluted with 0.3 mL/min of 10 mM sodium acetate buffer (pH 5.5) containing 0.1 M NaCl and 0.5 mM DTPA, and Griess reagent (0.15 mL/min) was added via a flow-reactor system. The diazo compound thus formed was detected at 540 nm by using a visible light detector (Eicom Company) and an integrator (System Instruments Company).

Ligand Binding

Ligand binding activities of HSA, SNO-HSA, and *S*-cGMP-HSA were determined by fluorescence measurements using the following site-specific probes: warfarin (site I; excitation: 320 nm, emission: 380 nm) and dansylsarcosine (DNSS, site II; excitation: 340 nm, emission: 476 nm). Within the limits of sensitivity, an excitation wavelength was chosen to give the maximum fluorescence of the probe bound to HSA, with insignificant fluorescence in the buffer. The concentration of the HSAs was 2 μM, whereas the total concentration of warfarin varied from 0.5 to 3 μM, and that for DNSS varied from 1 to 2.5 μM. The experiments were performed in PBS.

Antibacterial Activity

In vitro antibacterial activities of NO_2-cGMP, cGMP, *S*-guanylated cysteine (*S*-cGMP-Cys), and different protein preparations were examined according to previously reported methods, with slight modification.[13] We used M9 medium (pH 7.4) during incubation of bacteria with the potential antibacterial compounds. In brief, *Escherichia coli* American Type Culture Collection, *Salmonella typhimurium* LT2, *Pseudomonas aeruginosa*, *Klebsiella pneumoniae* MGH78578, *Bacillus subtilis*, *Streptococcus pyogenes*, *Streptococcus aureus* OM 481, and *S. aureus* OM 505 organisms were cultured overnight in M9 medium and were then washed three times with M9 medium. The bacteria were resuspended in Krebs–Ringer phosphate buffer containing 1 mg/mL NH_4Cl and 5 mg/mL thiamine hydrochloride. The bacterial suspensions (1×10^6 CFU/mL, 0.02 mL in M9 medium) were mixed with 0.18 mL of M9 medium containing different concentrations of the compounds being tested in a 96-well plate. After 1 h of incubation at 37°C, the bacteria were collected by centrifugation (1500*g*, 5 min), resuspended in 0.18 mL of M9 medium, transferred to another 96-well plate, and incubated for 9 h at 37°C. The numbers of bacteria present were determined by measuring the turbidity of the culture suspension: The A_{655} value was monitored by using a microplate reader (model 450; Bio-Rad Laboratories, Hercules, California).

Statistical Analysis

The statistical significance of collected data was evaluated using the ANOVA analysis followed by Newman–Keuls method for more than two means. Differences between groups were evaluated by the Student's *t*-test. A p value of less than 0.05 was regarded as statistically significant.

RESULTS AND DISCUSSION

Detection of Endogenous *S*-cGMP-Compounds in Human Plasmas

At first, we checked the specificity of the monoclonal *S*-cGMP antibody by Western blot analysis. Figure 1a

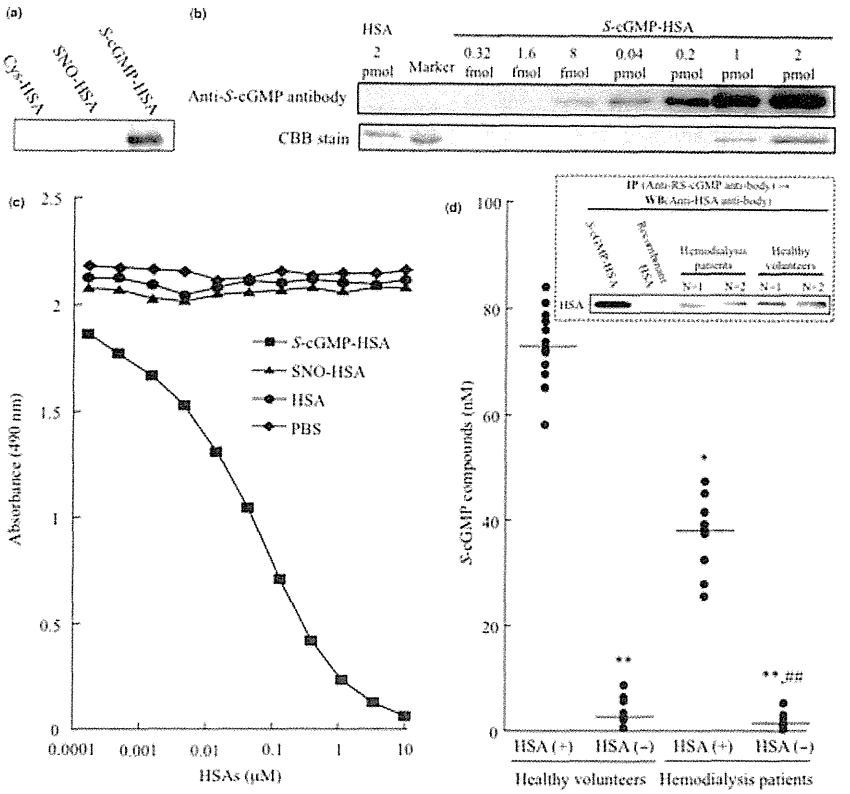

Figure 1. Quantitative evaluation of *S*-guanylated compounds in healthy volunteers and HD patients. (a) The specificity of a monoclonal anti-*S*-guanylated antibody against several HSAs. Cys-HSA, SNO-HSA, and *S*-cGMP-HSA were prepared *in vitro* (see the section *Material and Methods* for details). HSAs (10 ng of protein) were analyzed by using Western blotting with anti-8-RS-cGMP antibody. (b) The detection limit of *S*-cGMP-HSA by Western blotting analysis. *S*-cGMP-HSA (0.32 fmol–2 pmol of HSA) analyzed by using Western blotting with anti-8-RS-cGMP antibody (upper) and Coomassie brilliant blue (CBB) stain (lower). HSA (2 pmol) was used as a control, and bovine serum albumin was used as a marker. (c) A competitive curve of ELISA using anti-8-RS-cGMP antibody against PBS, HSA, SNO-HSA, and *S*-cGMP-HSA (see the section *Material and Methods* for details). (d) Quantitative analysis of *S*-guanylated compounds in intact human plasma, HSA(+), and in plasma without albumin, HSA(−), using the competitive ELISA method. HSA was removed by applying the plasma samples to a Blue Sepharose CL-6B (ϕ 2.5 × 20 cm^2) column.[15] (d, inset) The Western blotting analysis using polyclonal anti-HSA antibody after immunoprecipitation with monoclonal anti-8-RS-cGMP antibody of the *S*-cGMP adducts in the plasma. Data are expressed as means ± S.E.M. (n = 11–12). $^*p < 0.05$, $^{**}p < 0.01$ as compared with HSA (+) of healthy volunteers; $^{\#\#}p < 0.01$ as compared with HSA (+) of HD patients.

shows that monoclonal *S*-cGMP antibody reacted only with *S*-cGMP-HSA and not with Cys-HSA or SNO-HSA. The detection limit of *S*-cGMP-HSA by Western blot is about 8 fmol (Fig. 1b). Second, to detect endogenous *S*-cGMP compounds in human plasma, we constructed a quantitative competitive ELISA method using monoclonal *S*-cGMP antibody. As seen in Figure 1c, addition of HSA or SNO-HSA had no effect in this competitive ELISA. By contrast, our ELISA system competed with *S*-cGMP-HSA from nM range. By means of this ELISA system, we evaluated the presence of endogenous *S*-cGMP compounds in human plasma from healthy volunteers and HD patients. As shown in Figure 1d, the concentration of *S*-cGMP compounds in healthy volunteers is about two times higher than in plasma from HD patients (68 nM in healthy plasma vs. 34 nM in HD patients). Interestingly, after albumin removal, the *S*-cGMP compounds in both plasma were decreased very much and to the same level ($p = 0.25$). These findings propose that the majority of *S*-cGMP compounds is *S*-cGMP-HSA, and that *S*-guanylation of other proteins is not different between healthy volunteers and HD patients. To detect *S*-cGMP-HSA in the plasma more specifically, we performed a Western blot analysis, using polyclonal anti-HSA antibody, after immunoprecipitation with monoclonal anti-8-RS-cGMP antibody of the *S*-cGMP adducts in the plasma. These results also suggested

DOI 10.1002/jps

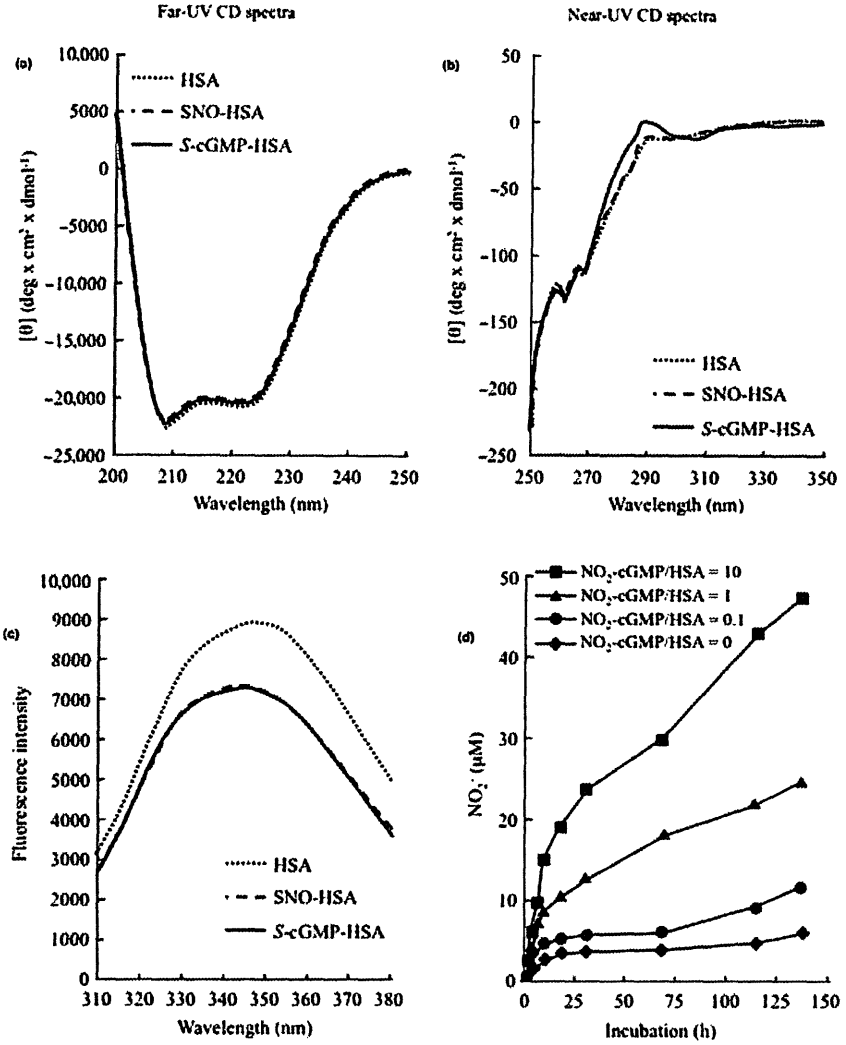

Figure 2. Structural integrity of HSA, SNO-HSA, and *S*-cGMP-HSA. Far-UV (a) and near-UV (b) CD spectra for HSA, SNO-HSA, and *S*-cGMP-HSA. (c) Intrinsic tryptophan fluorescence spectra of HSA, SNO-HSA, and *S*-cGMP-HSA excited at 295 nm were measured using a JASCO FP-777 spectrofluorometer. (d) Effect of different molar ratios of NO_2-cGMP on *S*-guanylation of HSA. Fifty micromolar DTT-treated HSA was incubated with 0–500 μM NO_2-cGMP for up to 5 days at 37°C. After each incubation, the mixtures were applied to a flow-reactor system. Data are expressed as means ± S.E.M. ($n = 4$).

that the majority of the *S*-cGMP compounds in human plasma is *S*-cGMP-HSA (Fig. 1d inset).

Physicochemical Characterization of *S*-cGMP-HSA

For studying the effect of *S*-guanylation on the physicochemical characteristics of HSA, we used CD spectroscopy (Figs. 2a and 2b) and intrinsic tryptophan fluorescence (Fig. 2c). According to the far-UV spectra, neither *S*-guanylation nor *S*-nitrosation of Cys-34 had any detectable effect on the secondary structure of native HSA (Fig. 2a). However, *S*-guanylation of the cysteine residue had a small effect on the tertiary structure of the protein (Fig. 2b). These minor conformational changes influence the tryptophan residue in position 214 because *S*-guanylation and *S*-nitrosation reduce tryptophan fluorescence (Fig. 2c). The spectral changes propose that the microenvironment of the residue has become more hydrophobic.

We have determined the efficiency of *S*-guanylation of HSA *in vitro*. For that purpose, HSA was incubated with different molar ratios of NO_2-cGMP for incubation times of up to 130 h. As seen in Figure 2d, *S*-cGMP-HSA was produced in a dose-dependent manner, and approximately 0.9 mol *S*-cGMP/mol HSA was formed after treatment of HSA with a 10 times molar excess of NO_2-cGMP for 130 h. According to a previous report, the efficiency of *S*-nitrosation of HSA by GS-NO was much lower, namely, 0.4 mol *S*-NO/mol HSA.[16] This indicates that HSA more readily becomes *S*-guanylated than *S*-nitrosated.

It has previously been shown that oxidation of Cys-34 decreased drug binding to both sites I and

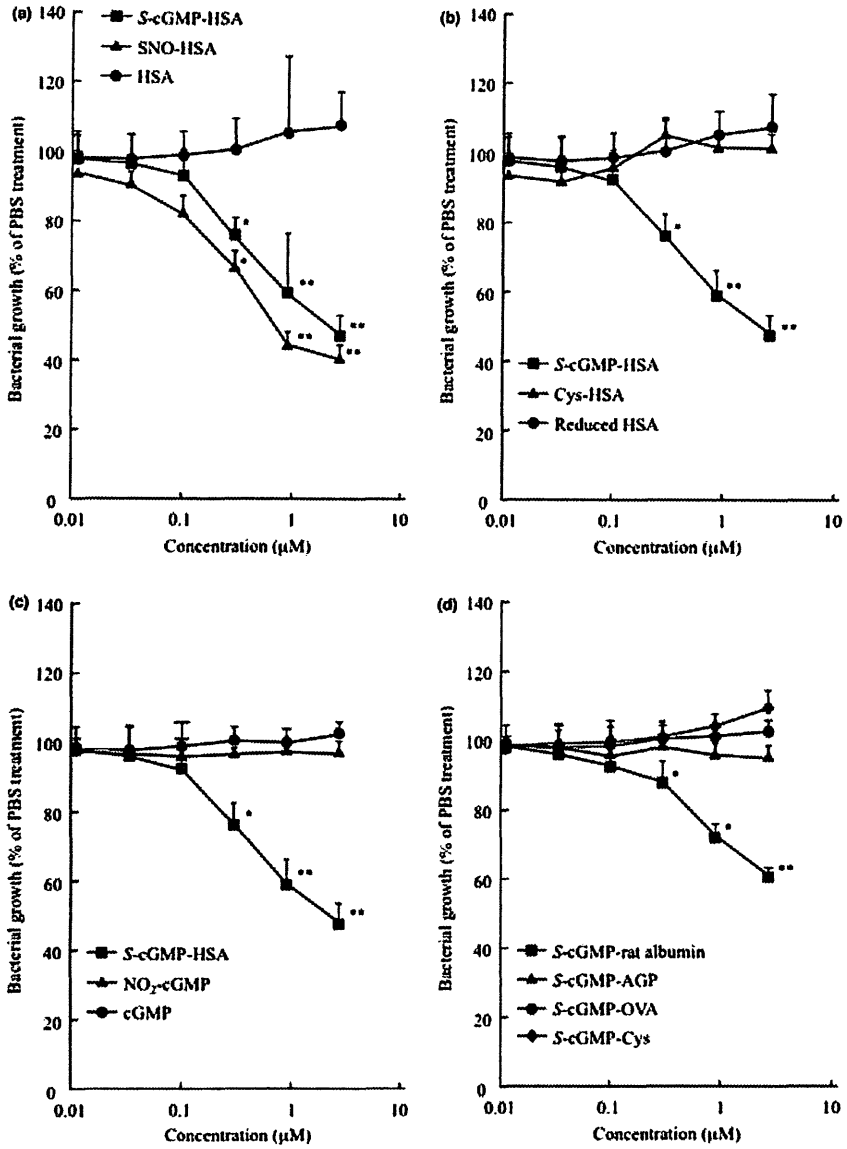

Figure 3. Concentration-dependent antibacterial effects of *S*-cGMP-HSA and related compounds. Bacterial growth, assessed by means of turbidity and expressed as a percentage of control, was determined at 9 h after incubation with the compounds indicated. Data are expressed as means ± S.E.M. ($n = 5$–7). $^{*}p < 0.05$, $^{**}p < 0.01$ as compared with bacterial growth in PBS.

II on HSA.[15] Therefore, we investigated whether *S*-guanylation also affected ligand binding to these two sites (Table 1). *S*-guanylation increased significantly the binding affinity of warfarin to site I, whereas DNSS binding to site II was not significantly changed. By contrast, *S*-nitrosation had no effect on binding of the two marker ligands. Taken together with the results of the spectroscopic studies, *S*-guanylation influences the structure of site I (which includes Trp-214) but apparently not that of site II in subdomain IIIA. In comparison, *S*-nitrosation has a smaller effect on the structure and function of HSA.

Table 1. High-Affinity Binding of Warfarin and DNSS to HSAs at pH 7.4 and 25°C

	Association Constant (10^5 M^{-1})	
HSAs	Warfarin	DNSS
HSA	3.77 ± 0.97	5.68 ± 0.98
S-cGMP-HSA	7.12 ± 0.65**	4.21 ± 1.13
SNO-HSA	3.72 ± 1.19	5.34 ± 0.81

HSAs concentration was 2 μM, whereas the total concentration of warfarin and DNSS varied from 0.5 to 3 μM and from 1 to 2.5 μM, respectively. The experiments were performed in phosphate buffered saline.

All values are mean ± S.E.M. ($n = 3$–6).

$^{**}p < 0.01$, compared with HSA.

DOI 10.1002/jps

Antibacterial Activity of S-cGMP-HSA

Nitric oxide and related species including RS-NO reportedly inhibit the growth of a wide variety of microorganisms, including viruses, bacteria, parasites, and fungi.[17] Miyamoto et al.[18] have shown that SNO-α_1-PI has a strong bacteriostatic effect against both Gram-negative and Gram-positive bacteria, with the half maximal inhibitory concentration (IC_{50}) in the low micromolar range. We have previously found that SNO-HSA has an antibacterial effect, with an IC_{50} value of 0.5–10 μM.[13] Therefore, we examined whether *S*-guanylation adds an antibacterial effect to HSA. In these experiments, SNO-HSA was used as a positive control. Interestingly, *S*-cGMP-HSA was as potent as SNO-HSA in suppressing bacterial growth, with an IC_{50} value of approximately 2 μM (Fig. 3a). On the contrary, parental HSA had no antibacterial activity. We have previously clarified that the antibacterial mechanism of SNO-HSA is caused by NO release from SNO-HSA.[13] However, the antibacterial effect of *S*-cGMP-HSA is not due to release of molecules or ions from the HSA complex (data not shown). We speculated whether oxidation of Cys-34 on HSA is involved in the antibacterial effect. Therefore, we studied the effect of Cys-34-reduced HSA (reduced-HSA) and Cys-HSA, but none of these compounds reduced bacterial growth (Fig. 3b). Furthermore, NO_2-cGMP and cGMP possess no antibacterial effect (Fig. 3c), suggesting that *S*-guanylation plays the important role for the antibacterial effect. Finally, we produced *S*-cGMP-Cys and several *S*-guanylated proteins using rat albumin, α-1 acid glycoprotein, and ovalbumin and measured bacterial growth in the presence of these *S*-guanylated compounds (Fig. 3d). The results show that only the modified rat albumin has an antibacterial effect, which, however, is less pronounced than that observed for *S*-cGMP-HSA. Thus, both *S*-guanylation and albumin seem to be necessary for the antibacterial effect. We have also measured the antibacterial activity of *S*-cGMP-HSA against other types of bacteria (Table 2). Among these, the IC_{50} value for *B. subtilis* was 300 nM. By contrast, the IC_{50} values for other bacteria types were higher than that for *E. coli*. Actually, it is difficult to explain the antibacterial activity of *S*-cGMP-HSA alone in human plasma. However, there are some antibacterial compounds in human plasma, for example, SNO-HSA, which exists at a concentration of around 7 μM in human plasma.[19] The present data suggest that *S*-cGMP-HSA is one of many endogenous antibacterial compounds. Most probably, these compounds "coordinately" act as antibacterial agents in the human body.

Table 2. Antibacterial Effects of *S*-cGMP-HSA Against Various Bacteria

	IC_{50} (μM)	
Gram Stain	*S*-cGMP-HSA	SNO-HSA
Negative		
E. coli	1.4	0.6
S. typhimurium LT2	100	8
P. aeruginosa	14	25
K. preumoniae MGH78578	9	1.3
Positive		
B. subtilis	0.3	0.17
S. pyogenes	100	10
S. aureus OM 481	100	100
S. aureus OM 505	100	100

CONCLUSION

Our study has two major findings. First, *S*-cGMP-HSA, a novel posttranslational modification of HSA, was detected in plasma from healthy volunteers and HD patients by quantitative competitive ELISA. HD resulted in a decrease in the concentration of *S*-cGMP-HSA from 68 ± 19 to 34 ± 22 nM. As judged from CD and fluorescence spectroscopy and from ligand binding studies, *S*-guanylation introduces only minor conformational changes in subdomain IIA of HSA, which contains Trp-214 and site I. Second, *S*-cGMP-HSA possesses an antibacterial activity *in vitro*, which is similar to that of SNO-HSA. These findings indicate that the risk of bacterial infection due to a low level of *S*-cGMP-HSA is increased during such a treatment and perhaps in pathological conditions as chronic kidney failure.[20]

S-cGMP-HSA most likely possesses the possibility for becoming an antibacterial agent of therapeutical use. Our data suggest that the antibacterial activity of *S*-cGMP-HSA is very similar to that of SNO-HSA. However, SNO-HSA has the drawbacks that it is very sensitive to light, metals, and reductants. 8-Nitro-cGMP has the advantage that it under physiological conditions irreversibly loses electrophilicity after *S*-guanylation; at least, so far, no specific catalyst has been found which can revert the process.[21] Our data suggest that *S*-cGMP-HSA can be regarded as an endogenous antibacterial agent and a useful new class of antibacterial agent with a circulation time sufficient for *in vivo* biological activity. On the basis of these advantages, we believe that further investigation in clinical settings is warranted.

ACKNOWLEDGMENTS

This research was supported by Grant-in-Aid for Scientific Research from the Japan Society for the Promotion of Science (KAKENHI 18390051 and 22790162). The work was also supported in part by grants from the Uehara Memorial Fund. We are grateful to Dr. Ayaka Suenaga and Ms. Fumika Yoshida at the Graduate School of Pharmaceutical Sciences, Kumamoto University, for helpful

discussions. Thanks are also due to members of the Gene Technology Center, Kumamoto University, for their important contributions to the experiments.

REFERENCES

1. Ignarro LJ, Kadowitz PJ, Baricos WH. 1981. Evidence that regulation of hepatic guanylate cyclase activity involves interactions between catalytic site -SH groups and both substrate and activator. Arch Biochem Biophys 208(1):75–86.
2. Ignarro LJ, Lippton H, Edwards JC, Baricos WH, Hyman AL, Kadowitz PJ, Gruetter CA. 1981. Mechanism of vascular smooth muscle relaxation by organic nitrates, nitrites, nitroprusside and nitric oxide: Evidence for the involvement of S-nitrosothiols as active intermediates. J Pharmacol Exp Ther 218(3):739–749.
3. Ignarro LJ, Barry BK, Gruetter DY, Edwards JC, Ohlstein EH, Gruetter CA, Baricos WH. 1980. Guanylate cyclase activation of nitroprusside and nitrosoguanidine is related to formation of S-nitrosothiol intermediates. Biochem Biophys Res Commun 94(1):93–100.
4. Hogg N. 2000. Biological chemistry and clinical potential of S-nitrosothiols. Free Radic Biol Med 28(10):1478–1486.
5. Foster MW, McMahon TJ, Stamler JS. 2003. S-nitrosylation in health and disease. Trends Mol Med 9(4):160–168.
6. Stamler JS, Simon DI, Osborne JA, Mullins ME, Jaraki O, Michel T, Singel DJ, Loscalzo J. 1992. S-nitrosylation of proteins with nitric oxide: Synthesis and characterization of biologically active compounds. Proc Natl Acad Sci USA 89(1):444–448.
7. Sawa T, Zaki MH, Okamoto T, Akuta T, Tokutomi Y, Kim-Mitsuyama S, Ihara H, Kobayashi A, Yamamoto M, Fujii S, Arimoto H, Akaike T. 2007. Protein S-guanylation by the biological signal 8-nitroguanosine 3′,5′-cyclic monophosphate. Nat Chem Biol 3(11):727–735.
8. Fujii S, Sawa T, Ihara H, Tong KI, Ida T, Okamoto T, Ahtesham AK, Ishima Y, Motohashi H, Yamamoto M, Akaike T. 2010. The critical role of nitric oxide signaling, via protein S-guanylation and nitrated cyclic GMP, in the antioxidant adaptive response. J Biol Chem 285(31):23970–23984.
9. Sawa T, Tatemichi M, Akaike T, Barbin A, Ohshima H. 2006. Analysis of urinary 8-nitroguanine, a marker of nitrative nucleic acid damage, by high-performance liquid chromatography-electrochemical detection coupled with immunoaffinity purification: Association with cigarette smoking. Free Radic Biol Med 40(4):711–720.
10. Peters T Jr. 1996. All about albumin: Biochemistry, genetics, and medical applications. San Diego, California: Academic Press.
11. Chen RF. 1967. Removal of fatty acids from serum albumin by charcoal treatment. J Biol Chem 242(2):173–181.
12. Ishima Y, Akaike T, Kragh-Hansen U, Hiroyama S, Sawa T, Suenaga A, Maruyama T, Kai T, Otagiri M. 2008. S-nitrosylated human serum albumin-mediated cytoprotective activity is enhanced by fatty acid binding. J Biol Chem 283(50):34966–34975.
13. Ishima Y, Sawa T, Kragh-Hansen U, Miyamoto Y, Matsushita S, Akaike T, Otagiri M. 2007. S-Nitrosylation of human variant albumin Liprizzi (R410C) confers potent antibacterial and cytoprotective properties. J Pharmacol Exp Ther 320(3):969–977.
14. Akaike T, Inoue K, Okamoto T, Nishino H, Otagiri M, Fujii S, Maeda H. 1997. Nanomolar quantification and identification of various nitrosothiols by high performance liquid chromatography coupled with flow reactors of metals and Griess reagent. J Biochem (Tokyo) 122(2):459–466.
15. Mera K, Anraku M, Kitamura K, Nakajou K, Maruyama T, Otagiri M. 2005. The structure and function of oxidized albumin in hemodialysis patients: Its role in elevated oxidative stress via neutrophil burst. Biochem Biophys Res Commun 334(4):1322–1328.
16. Ishima Y, Akaike T, Kragh-Hansen U, Hiroyama S, Sawa T, Maruyama T, Kai T, Otagiri M. 2007. Effects of endogenous ligands on the biological role of human serum albumin in S-nitrosylation. Biochem Biophys Res Commun 364(4):790–795.
17. Fang FC. 2004. Antimicrobial reactive oxygen and nitrogen species: Concepts and controversies. Nat Rev Microbiol 2(10):820–832.
18. Miyamoto Y, Akaike T, Alam MS, Inoue K, Hamamoto T, Ikebe N, Yoshitake J, Okamoto T, Maeda H. 2000. Novel functions of human alpha(1)-protease inhibitor after S-nitrosylation: Inhibition of cysteine protease and antibacterial activity. Biochem Biophys Res Commun 267(3):918–923.
19. Stamler JS, Jaraki O, Osborne J, Simon DI, Keaney J, Vita J, Singel D, Valeri CR, Loscalzo J. 1992. Nitric oxide circulates in mammalian plasma primarily as an S-nitroso adduct of serum albumin. Proc Natl Acad Sci USA 89(16):7674–7677.
20. Sarnak MJ, Jaber BL. 2000. Mortality caused by sepsis in patients with end-stage renal disease compared with the general population. Kidney Int 58(4):1758–1764.
21. Okamoto T, Khan S, Oyama K, Fujii S, Sawa T, Akaike T. 2010. A new paradigm for antimicrobial host defense mediated by a nitrated cyclic nucleotide. J Clin Biochem Nutr 46(1):14–19.

BJP British Journal of Pharmacology

DOI:10.1111/j.1476-5381.2011.01201.x
www.brjpharmacol.org

RESEARCH PAPER

Vascular responses to 8-nitro-cyclic GMP in non-diabetic and diabetic mice

Yoshiko Tokutomi[1,3], Keiichiro Kataoka[1], Eiichiro Yamamoto[1], Taishi Nakamura[1], Masaya Fukuda[1], Hisato Nako[1], Kensuke Toyama[1], Yi-Fei Dong[1], Khandaker Ahtesham Ahmed[2], Tomohiro Sawa[2], Takaaki Akaike[2] and Shokei Kim-Mitsuyama[1]

[1]*Department of Pharmacology and Molecular Therapeutics, Graduate School of Medical Sciences, Kumamoto University, Kumamoto, Japan,* [2]*Department of Microbiology, Graduate School of Medical Sciences, Kumamoto University, Kumamoto, Japan, and* [3]*Department of Nutritional Science, Faculty of Human Life Science, Shokei University, Kumamoto, Japan*

Correspondence
Professor Shokei Kim-Mitsuyama, Department of Pharmacology and Molecular Therapeutics, Graduate School of Medical Sciences, Kumamoto University, Honjo 1-1-1, Kumamoto 860-8556, Japan. E-mail: kimmitsu@gpo.kumamoto-u.ac.jp

Keywords
8-nitro-cGMP; vascular responses; aorta; db/db mouse; eNOS; superoxide anions

Received
20 February 2010
Revised
20 November 2010
Accepted
15 December 2010

BACKGROUND AND PURPOSE

8-Nitroguanosine 3′,5′-cyclic monophosphate (8-nitro-cGMP), formed nitric oxide (NO)-dependently, is a physiological second messenger, yet little is known about its role in the pathophysiology of vascular diseases. To study the pharmacological activity of 8-nitro-cGMP in diabetic mice, we compared its effects on vascular reactivity of aortas from non-diabetic and diabetic mice.

EXPERIMENTAL APPROACH

Vascular tension recording was performed in thoracic aortic rings from wild-type (C57BL/6), non-diabetic db/+ and obese/diabetic db/db mice. Endothelial NO synthase (eNOS) uncoupling and superoxide were tested by Western blot and dihydroethidium fluorescence respectively.

KEY RESULTS

8-Nitro-cGMP, at concentrations up to 10 μM, enhanced phenylephrine-induced contractions in aortas from C57BL/6 and db/+ mice, but not from db/db mice. This enhancement was not observed with 8-bromo-cGMP. Pretreatment of aortas from C57BL/6 and db/+ mice with L-NAME (100 μM), superoxide dismutase (100 $U \cdot mL^{-1}$) or tiron (1 mM), abolished 8-nitro-cGMP-induced enhancement of the phenylephrine contraction. In 8-nitro-cGMP (10 μM)-treated C57BL/6 aortas, eNOS dimer/monomer ratio was significantly decreased and vascular superoxide production increased, suggesting that 8-nitro-cGMP-induced superoxide production via eNOS uncoupling may mediate the enhancement of the phenylephrine contraction. At higher concentrations (>10 μM), 8-nitro-cGMP produced relaxation of the phenylephrine-contracted aortas from C57BL/6, db/+ and db/db mice. The 8-nitro-cGMP-induced relaxation in db/db mouse aortas was found to be resistant to a phosphodiesterase 5 inhibitor, zaprinast (1 μM).

CONCLUSIONS AND IMPLICATIONS

The vasodilator effect of 8-nitro-cGMP may contribute to amelioration of the vascular endothelial dysfunction in diabetic mice, representing a novel pharmacological approach to prevent the complications associated with diabetes.

Abbreviations

eNOS, endothelial nitric oxide synthase; L-NAME, N^{ω}-nitro-L-arginine methyl ester; 8-nitro-cGMP, 8-nitroguanosine 3′,5′-cyclic monophosphate; PDE, phosphodiesterase; PKG, protein kinase G; ROS, reactive oxygen species; SOD, superoxide dismutase

Introduction

Nitric oxide (NO) generated by endothelial nitric oxide synthase (eNOS) crucially determines vascular tone as well as vascular wall homeostasis. It is well established that NO stimulates cGMP production and induces subsequent signalling pathways in target cells. Recently, we discovered a nitrated derivative of cGMP, 8-nitro-cGMP, a novel second messenger that is formed nitric oxide synthase (NOS)-dependently in physiological systems and may be involved in redox activity and signal transduction by NO (Sawa *et al.*, 2007). This has led us to investigate a possible role of 8-nitro-cGMP in vascular function.

NO availability may be attenuated in part by reaction with reactive oxygen species (ROS), particularly superoxide ($\cdot O_2^-$) produced by oxidative stress in pathological conditions (Cai and Harrison, 2000; Vanhoutte *et al.*, 2009). Increased oxidative stress in vessel walls is an important element in the development and progression of diabetes and its complications (Baynes and Thorpe, 1999). Therefore, ROS scavenging has been proposed as a therapeutic strategy to target oxidative stress in vascular disorders. In addition, it was reported that overexpression of superoxide dismutase (SOD)-1 in type 2 diabetic db/db mice attenuates several indices of renal injury, possibly by inducing a reduction of peroxynitrite generation by NO–superoxide interaction (DeRubertis *et al.*, 2004).

Based on these findings, we hypothesized that 8-nitro-cGMP may play some role in the ROS-mediated pathophysiology of diabetic vascular dysfunction. To test this hypothesis, the present study was performed to examine the pharmacological activity of 8-nitro-cGMP in diabetic vessels, by comparing the effects of 8-nitro-cGMP on vascular responses of thoracic aortic rings from non-diabetic (C57BL/6 and db/+) and obese/diabetic (db/db) mice.

Methods

Animal experiments

Male BKS.Cg-Dock7^{m}+/+*Lepr*^{db}/J (db/db) mice, 13- to 14-week-old, age-matched littermates (db/+) and age-matched controls (C57BL/6) from The Jackson Laboratory (Bar Harbor, ME, USA) were used in this study. The animal protocol was approved by the Institutional Animal Care and Use Committee.

Aortic ring preparation and tension recording

The mice were killed by inhalation of diethyl ether and cervical dislocation and the thoracic aortas were excised immediately. Adventitial tissue was carefully removed. The aortic rings were mounted in a 3 mL organ bath chambers (MTOB-1, Labo Support, Osaka, Japan), filled with Krebs-Henseleit buffer (KHB, in mM: NaCl, 118.4; KCl, 4.7; $MgSO_4$, 1.2; KH_2PO_4, 1.2; $CaCl_2$, 2.5; $NaHCO_3$, 25; glucose, 10), bubbled with 95% O_2 and 5% CO_2, and maintained at 37°C. The rings were connected to a force transducer to measure isometric tensions and recorded on a transducer data acquisition system (PowerLab, Chart v5, AD Instruments, Colorado Springs, CO, USA). Resting tension was set at 1.0 g and rings were allowed to equilibrate for 60 min. KHB was changed before and twice after each concentration–response curve. Cumulative concentration–response curves for acetylcholine (ACh; 1 nM to 100 μM), 8-nitro-cGMP and 8-bromo-cGMP (1 nM to 300 μM) were generated after contraction of rings with an α_1-agonist, phenylephrine (Phe; 0.1 μM). All experiments for tension recording were conducted following induction of 20–30% of maximal Phe-induced contraction, to get a significant response to 8-nitro-cGMP or 8-bromo-cGMP. All inhibitors/scavengers used in this study were allowed to incubate with the preparation for 30 min before the construction of the concentration–response curve.

Detection of eNOS dimer disruption and superoxide production

For measurements of eNOS dimer/monomer ratio and *in situ* superoxide production, the isolated aortas were treated with 8-nitro-cGMP or 8-bromo-cGMP as follows: isolated mice aortas were removed, cleared of connective tissue and immersed in warm KHB (37°C) for equilibration for 90 min. Subsequently, vessel segments were incubated for 30 min in control KHB or in KHB containing 8-nitro-cGMP or 8-bromo-cGMP. The segments were then snap-frozen at –80°C for immunoblotting and dihydroethidium (DHE) staining.

For immunoblotting, homogenates of thoracic aorta were prepared from the frozen segments in lysis buffer containing 50 mM Tris-HCl (pH 7.4), 150 mM NaCl, 0.5% Triton X-100 and protease inhibitors. Protein concentrations were determined using BCA protein assay kit (Pierce, Rockford, IL, USA). Aortic eNOS dimer and monomer were separated, using low-temperature SDS-PAGE followed by Western blot analysis, as described in our previous study (Yamamoto *et al.*, 2007a). In brief, protein extracts were mixed with fivefold SDS sample buffer (0.31 M Tris-HCl, pH 6.8, 10% SDS, 50% glycerol, 0.5 M dithiothreitol and 0.03% bromophenol blue) at 0°C. Electrophoresis was performed in a cold room (4°C). eNOS dimer and monomer were detected with anti-eNOS antibody (1:2000, BD Biosciences, Lexington, KY, USA). The immunoreactivity was detected by enhanced chemiluminescence method (ECL; GE Healthcare Bioscience, Piscataway, NJ, USA) and quantified using a luminescence image analyser LAS-4000mini and image analysis software Multi Gauge Ver.3.11 (Fuji Film, Tokyo, Japan).

In situ superoxide production was determined in vessel cryosections with the oxidative fluorescent dye DHE, as previously described (Yamamoto *et al.*, 2007b; Nakamura *et al.*, 2009). Cryosections (8 μm in thickness; Leica, Weltzar, Germany) from the aortas treated with 8-nitro-cGMP or 8-bromo-cGMP were incubated with DHE (5 μM) at 37°C for 30 min and then viewed by fluorescent microscopy (Nikon, Eclips, Tokyo, Japan). For each slide, at least five images from different sections of the slide were captured, and average staining intensity was calculated using image analysis software (Lumina Vision version 2.2, Mitani-Corp., Fukui, Japan).

Data analysis

Relaxation responses are expressed as a percentage reversal of the Phe-induced contraction. Responses are plotted graphically as means from at least four separate experiments with vertical bars representing SEM. Curves were fitted to all the